Journal of Materials Chemistry A

PAPER

View Article Online
View Journal | View Issue

Cite this: J. Mater. Chem. A, 2017, 5, 1248

Degradation of radiation grafted hydroxide anion exchange membrane immersed in neutral pH: removal of vinylbenzyl trimethylammonium hydroxide due to oxidation

Richard Espiritu,[ab] Bernard T. Golding,[c] Keith Scott[a] and Mohamed Mamlouk*[a]

Received 22nd September 2016
Accepted 11th December 2016

DOI: 10.1039/c6ta08232g

www.rsc.org/MaterialsA

Anion exchange membranes (AEMs) fabricated using polyethylene (PE) and ethylene tetrafluoroethylene films are subjected to degradation tests in deionised water for electrolyser/fuel cell operation. After the degradation test, the decrease in ion-exchange capacity (IEC) of the AEM, hence decrease in ionic conductivity, is found to be influenced by the applied gamma radiation dose rate. The use of high radiation dose rate produces membranes with improved stability in terms of % IEC loss due to shorter, more uniformly distributed vinylbenzyl chloride (VBC) grafts. For LDPE-based AEMs, increasing the applied radiation dose rate during grafting from 30 to 2000 Gy h^{-1} significantly reduces AEM % IEC loss from 38 to 11%, respectively. Analyses of both the aged functionalised membranes and their resulting degradation products confirm the loss of not only the functional group, but also the VBC group, which have not been reported previously in the literature. Oxidation reactions taking place in solutions close to neutral can be the main contributor to the IEC loss in contrast to the widely reported E2 or SN2 attack on the head group in high alkalinity solutions. We therefore propose parallel degradation mechanisms to head group loss of AEM that involves peroxide radicals which is more dominant at low alkalinity solutions.

1. Introduction

Among the different types of fuel cell systems, proton-exchange membrane fuel cells (PEMFCs) and alkaline fuel cells (AFCs) are the most studied for practical service applications, particularly in low temperature regimes of operating conditions. With the development of solid anion-exchange membranes (AEMs), working in alkaline anion-exchange membrane environment (AAEM) has several advantages over proton exchange membrane environment (PEM) for fuel cell and water electrolyser (PEMWE), namely, faster oxygen reduction reaction (ORR) and oxygen evolution reaction (OER) under alkaline conditions than in their acidic counterpart therefore providing lower activation losses,[1,2] feasible use of non-noble metal catalysts[3–5] and cheaper cell components due to a less corrosive environment.[6,7] Furthermore, with the use of solid AEM, electrolyte leaking and carbonate precipitation are prevented due to the effective separation of the fuel and the oxidant[8] which also allow operation under differential pressure across the membrane.

Alkaline AEMs are solid polymer electrolytes that contain positive ionic groups, typically quaternary ammonium groups: $-N^{+}(CH_3)_3$, and mobile negatively charged anions, usually OH^{-}.[9,10] There have been several classes of AEMs fabricated for AFC operations reported in literature. The most common class of AEMs is those based on quaternary ammonium groups[11,12] due to their appreciable stability in an alkaline environment.[13,14]

We have reported the ionic conductivity and fuel cell performance of several benzylammonium and sulfonium head groups for AEMs and found that trimethylamine (TMA)-functionalised ionomers showed superior ORR performance and higher ionic conductivities in comparison to other studied head groups including 1,4-diazabicyclo[2.2.2]octane (DABCO).[10,15] Our report[2] showed an increase of around 60% of the power density at 0.4 V when TMA was used instead of *N*,*N*,*N*′,*N*′-tetramethyl-1,6-hexanediamine (TMHDA) at 60 °C. Furthermore, TMA-functionalised vinylbenzyl chloride (radiation) grafted on low-density polyethylene backbone (LDPE-*g*-VBC-TMA) showed low activation energy of 12 kJ mol^{-1} for OH^{-} ionic conductivity[2] close to the reported value for H^{+} conductivity in Nafion[3] with OH^{-} through plane conductivity of 0.13 S cm^{-1} at 80 °C and 100% RH.[2] These (LDPE-*g*-VBC-TMA) AEMs have superior fuel cell peak power densities at a high potential of 500 mV, one of the highest reported in the literature for AAEMFCs of 823 mW cm^{-2} under oxygen (atm) and 506 mW cm^{-2} under air (1 bar gauge) at 60 °C.[16]

[a]School of Chemical Engineering and Advanced Materials, Merz Court, Newcastle University, Newcastle upon Tyne, NE1 7RU, UK. E-mail: mohamed.mamlouk@ncl.ac.uk

[b]Department of Mining, Metallurgical and Materials Engineering, University of the Philippines Diliman, Quezon City 1101, Philippines

[c]School of Chemistry, Bedson Building, Newcastle University, Newcastle upon Tyne, NE1 7RU, UK

While AEMFCs has shown excellent ionic conductivity and cell performance, their chemical and thermal stability for long term service life remains a challenge. Alkaline stability and degradation of AEMs are mainly assessed in the purview of cation stability. The literature has abundantly discussed mechanisms of the degradation of AEMs, namely, Hofmann elimination, nucleophilic substitution and formation of ylide derivatives.[17–26] Hofmann elimination is when OH^- ions attack a β-hydrogen atom (with respect to N) of the cation which leads to the elimination of a tertiary amine from the neighbouring carbon.[18,20,21] Nucleophilic substitution involves OH^- ions acting as a strong nucleophile, which can either (1) attack the α-carbon atom of the cation converting the quaternary ammonium group to a tertiary amine and releasing an alcohol or (2) attack the benzylic carbon atom causing the detachment of a tertiary amine.[19,22,24] Lastly, the ylide formation route is through OH^- ions abstracting a proton (α-hydrogen) from a methyl group producing a nitrogen ylide intermediate which transforms to tertiary amine and water.[23,25,26] These ylide intermediates can further undergo degradation through the Stevens rearrangement or Sommelet–Hauser mechanism,[17,27–29] selectivity of which is dependent on the electronic properties of the substituents attached to the aromatic ring, steric effects and the type of solvent used.[29] These three degradation mechanisms can occur in parallel, which can lead to a combination of degradation products. It is thus important to synthesise membranes with chemical structures capable of circumventing these degradation mechanisms to ensure long term stability of AEMs.

The chemical and thermal stability of AEMs greatly depend on the nature of the polymer backbone and on the type of functional group that enables the transfer of hydroxide ions.[30] The use of hydrocarbon-based polymer backbones, like polyether sulfone (PES) and polyphenylene oxide (PPO), for AEMs offer advantages, namely, low cost, commercial availability and structures that are amenable for tethering pendant groups.[31] However, even though PES-based AEMs are tolerant to highly basic environment, the polymer backbone gradually degrades in alkaline medium when quaternised with ammonium functional group.[22,32] The PPO-based AEM, on the other hand, undergoes backbone degradation by chain scission *via* hydrolysis of ether bonds.[33,34] The fluorinated base polymers have emerged to be the preferred polymer backbone for AEM preparation owing to its inherent inert properties and electrochemical and thermal stability due to the presence of strong electron-withdrawing fluorine atom.[35] However, it has been reported that partially fluorinated polymers like PVDF-based AEMs are known to degrade in alkaline media *via* dehydrofluorination.[36,37]

The fact that novel fluorocarbon-type AEMs are still unstable under strong basic conditions[6,38] suggests that the functional ion-exchange groups rather than the cross-linked polymer network undergoes degradation. Therefore, it can be assumed that the alkaline stability of an AEM is given by the stability of the weakest link, which is generally considered to be the head group. Among the different type of positive ionic groups, the quaternary ammonium ions possess a considerably higher thermal and chemical stability compared to phosphonium or sulfonium groups.[20] However, it was reported that phosphonium groups have demonstrated their potential by exhibiting greater stability towards attack by hydroxide ion than the more conventional quaternary ammonium.[39]

The attachment of the head group to the polymer backbone can be typically achieved through benzyl or phenyl bonds. Benzyl-trimethylammonium (benzyl-TMA) is far more stable than its phenyl equivalent.[14] 90% of benzyl-TMA was found to be stable after 29 days alkaline treatment compared to only 30% for phenyl-TMA.[25] Among the several studied quaternary ammonium head groups, benzyl-TMA and benzyl-DABCO showed the highest stability in 2 M KOH at 160 °C (under N_2) with half-time disintegration of 29 and 42 min, respectively.[40]

The chemical stability of AEMs in the OH^- form, particularly at high temperatures, poses a critical challenge that limits the wide scale use of AEMFCs. In our previous publication,[41] we have successfully demonstrated the long term stability of the fabricated polyethylene-based AEMs for AAEMFCs operating at temperature of up to 80 °C. We have shown that the degradation rate is strongly dependent on oxidant concentration, where degradation rate under oxygen (atm) was more than 4 times faster than that under nitrogen. However, limited chemical analysis has been conducted regarding the chemical stability of AEMs. Thus, a more fundamental understanding of the chemical stability of AEMs is required to adequately design robust solid-state AEMFCs and electrolysers.[23] Degradation tests of membranes having quaternary ammonium groups reported in literature were all performed in high alkaline concentrations[42,43] and elevated temperature.[14,23,44] This study is the first attempt to illustrate the degradation of the OH^- exchanged AEM stored in deionised water, which is the usual medium present in electrolyser and fuel cell operations. Furthermore, the majority of the published work assessed membrane stability by measuring the decrease in its weight, ion exchange capacity and ionic conductivity with time.[23,42,43,45–49] However, very limited research has been done to analyse the decomposition products. This is partially due to the insoluble nature of some of these products,[50] limiting the techniques available for chemical analysis needed to identify their structure. Due to such difficulties, we have gathered results from several chemical analyses to determine the identity of the degradation products. Most importantly, all of the available literature have so far reported that the degradation of AEMs is due to the removal of the ion-carrying functional groups and not the graft VBC.[6,11,13,19,20,40,51,52] This research is the first to report that the degradation of the AEMs is not only due to the removal of the functional group, but also attributed to the loss of the benzene ring, in the AEMs we have synthesised and investigated. Such findings will have a significant impact on the way we design and fabricate AEMs in order to obtain excellent thermal and chemical stability properties.

2. Mechanism of AEM degradation

For the TMA-functionalised membranes, the attachment of TMA to the benzylic chloride during functionalisation does not produce β-hydrogens, thus the Hofmann elimination route can be conveniently disregarded.[43,49,53] When the Hofmann

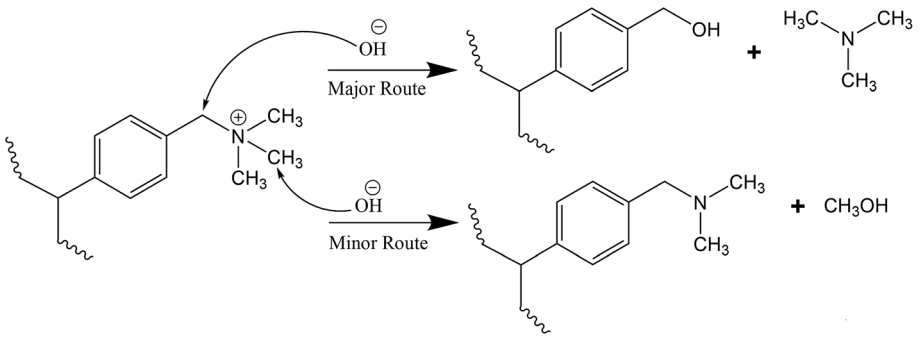

Scheme 1 Degradation mechanism of OH^- ion attack on TMA cation group *via* nucleophilic substitution.[54]

elimination is impossible, nucleophilic substitution proceeds preferably towards the release of TMA rather than producing the benzyl-dimethylamine unit[23,40,54] as shown in Scheme 1. This is because nucleophilic substitution reaction is generally favourable at a benzylic methylene carbon and TMA is a good leaving group.[55,56] The reaction consequently leaves behind a benzylic alcohol[54] that could readily transforms to dibenzylic ether, and together with TMA, are the major decomposition products.[57]

Stevens rearrangement for the benzyl-TMA group in basic media involves abstraction of the relatively acidic proton from the methylene group connecting the aromatic group and the TMA to form an ylide. This ylide intermediate undergoes rearrangement to produce a tertiary amine and water as final products (Scheme 2).[28] Similar to the Stevens rearrangement, the Sommelet–Hauser mechanism also involves proton abstraction by OH^- ions, however the attack is on a methyl group attached to the quaternary nitrogen atom and the resulting carbanion attacks the *ortho*-position of the aromatic ring (Scheme 2).[29]

For the benzyl-TMA cation, Stevens rearrangement is the only ylide reaction observed as the OH^- ion prefers the proton attached to the methylene group connecting the aromatic ring and the TMA, rather than a methyl attached to the quaternary nitrogen atom.[27,28] However, recent studies have suggested that this ylide reaction pathway is reversible and does not lead to cation degradation,[13,26,46,58] while DFT calculations suggest that both pathways (ylide formation and OH^- attack) have the same overall barrier[25] and in close to neutral pH (low OH^- concentration) it is expected that the ylide formation will be more dominant.

Unlike the TMA-functionalised membranes, the reaction between DABCO and VBC results in the presence of β-carbons.

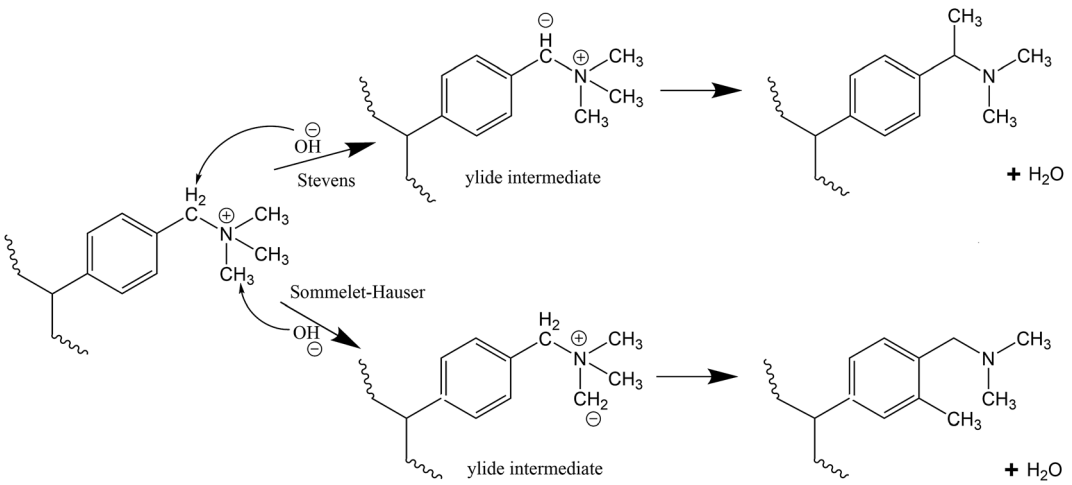

Scheme 2 Stevens rearrangement[56] and Sommelet–Hauser mechanism[59] for the benzyl-TMA cation group.

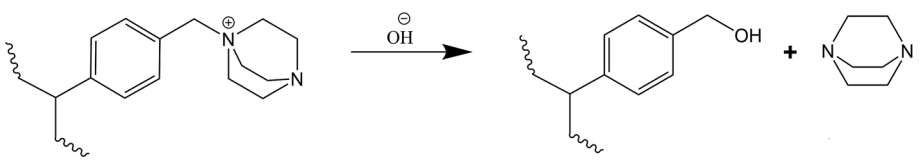

Scheme 3 Degradation mechanism by nucleophilic substitution of OH^- ion on the methylene group attached to DABCO.[40]

Even though DABCO has β-hydrogens, its structure does not allow the stereoelectronics necessary for a Hofmann elimination mechanism.[19,21,24] However, the mono-quaternised DABCO can undergo a nucleophilic displacement reaction causing the release of DABCO to the solution as shown in Scheme 3.[23,40]

3. Experimental

3.1 Materials

The low-density polyethylene films were sourced from British Polythene Industries plc. The ethylene-tetrafluoroethylene films were procured from Nowoflon Kunststoffprodukte GmbH while the high-density polyethylene films were obtained from Metal Box Co. All commercial polymer films were used as received. Vinylbenzyl chloride (mixture of 3- and 4-isomers, 97%), trimethylamine (45% in water) and 1,4-diazabicyclo[2.2.2]octane were all acquired from Sigma-Aldrich. Toluene solvent, potassium hydroxide pellets, acetone, sulfuric acid, methanol and sodium chloride were all analytical reagent grade and were used as received.

3.2 Anion exchange membrane preparation

The AEMs were synthesised as previously reported[16,41] using low-density polyethylene (LDPE), high-density polyethylene (HDPE) and ethylene-tetrafluoroethylene (ETFE) as base polymers with vinylbenzyl chloride (VBC) as the graft monomer. The PE-*g*-VBC copolymer was prepared by immersing the PE films in nitrogen purged 31/26/45 by volume VBC/toluene/methanol solution placed in a screw-cap vial. Samples were sent to Synergy Health plc (Wiltshire, UK) for mutual gamma radiation grafting. The irradiation was carried out under known dose rate and total radiation dose for a predetermined time. On the other hand, the ETFE-*g*-VBC membrane was produced by irradiating first the ETFE film using an electron-beam source (4.5 MeV) to a total radiation dose of 70 kGy and was subsequently immersed in N_2-purged VBC monomer solution. The grafted membranes obtained were washed thoroughly with acetone to completely remove VBC homopolymers. To produce the AEM, trimethylamine (TMA) was used to impart functionality to the PE-*g*-VBC (Scheme 4) and ETFE-*g*-VBC copolymers. Another set of LDPE-based membranes was prepared but functionalised with DABCO. Scheme 4 shows an idealised schematic of the preparation of polyethylene-based AEM functionalised with TMA.

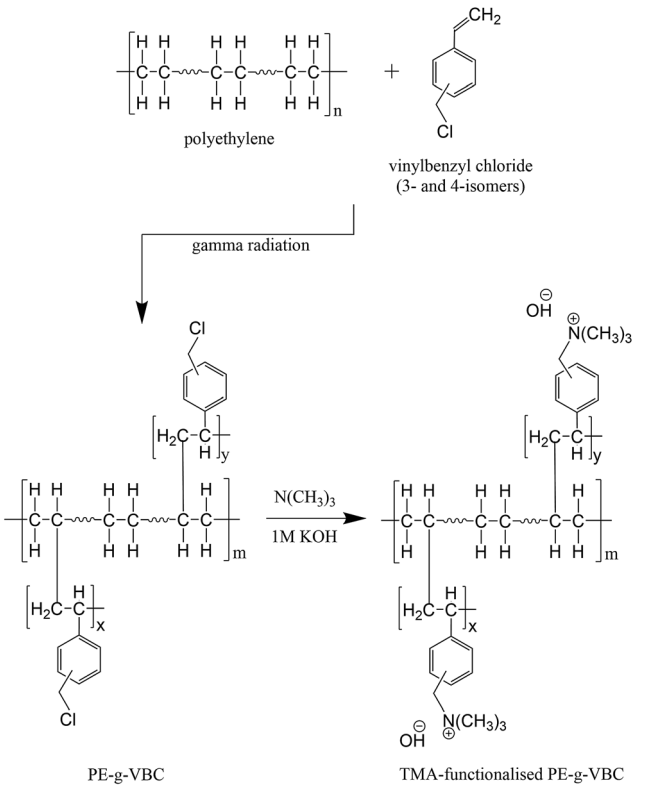

Scheme 4 Representative schematic of polyethylene-based AEM synthesis.[41]

3.3 Membrane stability tests

3.3.1 Stability test of un-exchanged LDPE-based AEM. The stability of unexchanged TMA- and DABCO-functionalised LDPE-*g*-VBC copolymer membrane (Cl form) was studied in air-saturated (CO_2 free) deionised water in sealed bottles and were placed inside a water bath at 60 °C for 3 months for comparison.

3.3.2 Stability test of OH^- exchanged functionalised AEMs. Functionalised AEMs were treated with 1.0 M KOH solution for 20 min. The solution was replaced with fresh 1.0 M KOH solution and the process was repeated until a total OH^- exchange time of 1 h was achieved to ensure complete exchange of chloride ions to hydroxide ions. The membrane was washed with copious amount of deionised water to remove residual hydroxide ions. Removal of excess OH^- ions was confirmed by using pH paper. OH^- exchanged membranes were placed in sealed bottles immersed in air-saturated (CO_2 free) deionised water and were secured in a water bath. Stability tests were performed with varying temperature and degradation time.

After the stability tests, the sealed bottles were allowed to cool to room temperature and the aged membranes were extracted and analysed separately. The degradation solutions, on the other hand, were visually examined and presence of suspended solid precipitates were separated from the solution using Eppendorf 5804R Centrifuge. The clear solution was then allowed to dry at 50 °C using a MTI Model DZF-6020-FP vacuum oven for recovery of solid precipitates.

3.4 Characterisation of the membrane and the degradation products

3.4.1 Measurement of the ion-exchange capacity (IEC). The OH^- exchanged membranes were immersed in a known volume of 1.0 M NaCl solution and was left to stand overnight. The liberated hydroxide ions were titrated with 0.10 M H_2SO_4 solution using a Titrette GMBH bottle-top digital burette and the endpoint was determined visually using methyl red indicator. After titration, the membranes were washed with deionised water to completely remove the salt and dried using a MTI Model DZF-6020-FP vacuum oven. Measurements of the weight were performed until no change in the dry weight was achieved.

The IECs were computed using the amount of OH^- ions neutralised, expressed in mmol, divided by the dry weight of the membranes, in grams.

3.4.2 Measurement of the ionic conductivity. Each OH^- exchanged membrane was sandwiched between two Freudenberg FCCT H2315-C2 gas diffusion layer carbon electrodes and was placed in a gold-plated titanium test cell. The environment inside the test cell was maintained at atmospheric pressure and the humidifier temperature was set to ensure 100% relative humidity inside the cell, which was verified using a Vaisala HUMICAP humidity sensor. The through-plane conductivity was measured using a two-point technique with each probe placed on either side of the membrane (through plane). The impedance was measured using a N4L NumetriQ PSM 1735 Frequency Response Analyser within the frequency range of 200 to 20 kHz with perturbation voltage amplitude of 15 mV. Three readings of the impedance in 5 min intervals were made and the average was determined. Consequently, the conductivity of the membrane was computed based on the following formula:

$$\sigma = \frac{4L}{R(\pi d^2)} \quad (1)$$

where σ is the hydroxide ion conductivity, L is the membrane thickness, R is the resistance derived from the impedance value at zero-phase angle and d is the diameter of the membrane test area.

3.4.3 Chemical analysis. The following sections describe the equipment utilised to characterise the membrane before and after the stability test and the resulting degradation products.

3.4.3.1 SEM analysis. Scanning electron microscopy (SEM) coupled with Energy-dispersive X-ray spectroscopy (EDX) was performed using a JEOL JSM-5300LV machine equipped with RONTEC UHV Dewar Detector.

3.4.3.2 Nuclear Magnetic Resonance (NMR) spectroscopy. Solid-state (^{13}C and ^{15}N) NMR analysis employing magic-angle spinning with cross-polarisation (CP-MAS) of the AEMs before and after degradation and the resulting degradation products were performed using tetramethylsilane and nitromethane as chemical shift references, respectively. For the solid-state ^{17}O NMR analysis of the membrane, direct-excitation (DE-MAS) was employed with water as the chemical shift reference. All solid-state (^{13}C, ^{15}N and ^{17}O) NMR spectra obtained with two-pulse phase-modulated (TPPM) decoupling were acquired using a Varian VNMRS Spectrometer at the EPSRC National Solid-State NMR Service in Durham University, UK. The enriched water–^{17}O (70–75.9 atom% ^{17}O, Aldrich) was used to prepare 0.1 M NaOH solution in a glove box by adding appropriate amount of Na. The membrane was immersed in this solution for 2 months at 60 °C. The membrane was rinsed with deionised water and dried in air in a vacuum oven at 50 °C. The isotope-labelled degradation solution was subjected to solution NMR analysis using a Bruker 500 Avance III HD spectrometer to obtain the ^{17}O NMR spectra.

3.4.3.3 Fourier-transform infrared (FTIR) spectroscopy. Determination of chemical structure and presence of functional groups were performed using a Varian 800 FT-IR Spectrometer with scan range of 4000 to 500 cm^{-1} equipped with a Pike Technologies diamond crystal plate Attenuated Total Reflectance (ATR) unit.

4. Results and discussion

4.1 Stability of LDPE-*g*-VBC copolymer and the fabricated membrane

The stability of the fabricated membranes was assessed by measuring the IEC of the un-exchanged (Cl^- form) membranes before and after immersing the membranes in deionised water at 60 °C for 3 months. Table 1 indicates the stability of the synthesised membranes having the same degree of grafting (DOG) wherein IEC did not change after the stability test. Both the DABCO- and TMA-functionalised membranes in their unexchanged (Cl^-) forms were found to be stable at 60 °C for 3 months with no change in their IEC. The solutions wherein the membranes were immersed were also oven dried and no solid precipitates were recovered indicating that there was no soluble degradation products of the membrane.

4.2 Effect of radiation dose rate

Table 2 shows the summary of the grafting conditions (radiation source, total dose and dose rate), DOG and IEC of the fabricated membranes using different base polymer (LDPE, HDPE and ETFE), with their respective membrane codes, and all of them functionalised with TMA. The IEC of the OH^- exchanged aged TMA-functionalised membranes were measured after 2 months and compared to their initial IECs as further shown in Table 2. The initial IECs of the membranes varied as expected based on their DOG for each type of base polymer. The resulting DOG upon grafting is influenced by the applied dose rate and total radiation dose. With all of the other parameters remaining constant (*i.e.* VBC monomer concentration, amination time, and total radiation dose), higher dose rate results in a higher DOG as more high energy radiation is supplied to grafting,[41] which is observed in LDPE and HDPE (Table 2). The IEC of the membrane decreased after 2 months of

Table 1 The IEC of fabricated membranes (Cl^- form) immersed in deionised water at 60 °C

				IEC (mmol g^{-1})	
Membrane code	Radiation dose rate (Gy h^{-1})	DOG (%)	Functionality	Initial	After 3 months
LD-1	2000	65.5	DABCO-functionalised	2.2 ± 0.1	2.2 ± 0.1
LT-1			TMA-functionalised	2.8 ± 0.2	2.8 ± 0.2

Table 2 A summary of the membrane codes and radiation grafting conditions for fabrication of TMA-functionalised AEMs with different base polymers and their IECs after stability test at 60 °C

Membrane code	Radiation source	Base polymer	Total dose (kGy)	Dose rate (Gy h^{-1})	DOG (%)	IEC (mmol g^{-1})		
						Initial	After month 2	IEC loss (%)
LT-2	Gamma radiation	LDPE	10	30	32	1.6 ± 0.1	1.0 ± 0.1	37.5
LT-3			10	35	58	2.4 ± 0.2	1.6 ± 0.1	33.3
LT-4			10	67	68	2.8 ± 0.2	2.2 ± 0.1	21.4
LT-1			20	2000	65	2.7 ± 0.2	2.4 ± 0.2	11.1
HT-1		HDPE	10	30	27	1.4 ± 0.1	0.7 ± 0.1	50.0
HT-2				35	58	2.6 ± 0.2	1.4 ± 0.1	46.2
HT-3				67	66	2.9 ± 0.3	2.1 ± 0.1	27.6
ET-1	Electron beam	ETFE	70	400	29	1.3 ± 0.1	1.1 ± 0.1	15.4
ET-2					37	1.5 ± 0.1	1.3 ± 0.1	13.3

soaking in deionised water at 60 °C for all types of OH^- exchanged AEM investigated. Such a decrease in IEC is an indication of the loss of the functional groups that enable the transfer of charge. The data further demonstrates that AEM with higher DOG exhibits slower degradation in terms of % IEC loss compared to that of AEM with lower DOG having the same type of base polymer. This suggests that the degradation rate is limited by factors other than the functional group concentration (IEC). This further suggests that there is a stability benefit as well as conductivity benefit from the use of membrane with high DOG for electrolyser/fuel cell application that is operating at a very low alkaline concentration.

The differences obtained in membrane DOGs are the direct result of the influence of the applied radiation dose rate (at the same total dose) during mutual radiation grafting. It can be observed that the variation in % IEC loss is directly related to the dose rate used. For example, LDPE-based AEM with a dose rate of 30 (LT-2), 35 (LT-3) and 67 Gy h^{-1} (LT-4), exhibited % IEC loss after 2 months of 37, 33 and 21%, respectively. Similarly with the HDPE-based AEM, at dose rate of 30 (HT-1), 35 (HT-2) and 67 Gy h^{-1} (HT-3), the % IEC loss observed after 2 months was 50, 46 and 28%, respectively. This leads to the conclusion that subjecting the base polymer to a higher dose rate will lead to a slower rate of degradation and hence to a more stable membrane. Lower dose rates can cause oxidative degradation to the base polymer, which decreases the extent of crosslinking compared to subjecting the base polymer to high dose rates which is normally favourable.[60,61] High dose rate treatment increases the degree of crosslinking of the base polymer, which provides structural strength and stability to the AEM.[62,63] When polymers are exposed to ionising radiation, even at low doses, they often undergo structural changes accompanied by molecular cross-linking, grafting and chain-scission reaction. It should however be mentioned that the highest total radiation dose (70 kGy for ETFE and 20 kGy for LDPE) used to fabricate the AEMs is still relatively low to cause substantial damage to the base polymer structure[64–66] and was confirmed previously by FTIR.[41] Furthermore, subjecting the polymer to high dose rate quickly consumes available oxygen and thus effectively prevents any dissolved oxygen from penetrating into the polymer and causing undesirable side reactions as the time of high energy application is so short.[60,67] Expectedly, when radiation grafting was performed with a very high dose rate of 2000 Gy h^{-1}, the AEM stability further improved with only 11% IEC loss over a 2 months test.

Another important factor that should be considered is the effect of dose rate on the distribution and the length of VBC chains in the grafted polymer. Ideally during simultaneous radiation grafting, each VBC unit should be attached to each of the polyethylene chain upon creation of a free radical leading to very short length graft (Scheme 5a). However, there is a competition between the grafting process and the VBC polymerisation. After the initial VBC unit attached itself to the polyethylene backbone, subsequent VBC units attach to the VBC unit (VBC polymerisation) instead of the polyethylene chain resulting in longer grafts (Scheme 5b). Using higher dose rates will result in faster decay of radicals by recombination and consequently faster termination of the growing VBC chains. This results in a shorter VBC grafted chains due to a decrease in styrene concentration in the internal grafting layers.[68,69] While at slow dose rates, VBC diffusion through the base polymer is sufficiently fast and the lifetime of the radicals formed is long enough to result in longer and fewer VBC chain grafts[70] *i.e.* faster dose rates will result in better distributed VBC throughout the grafted polymer and more LDPE–VBC links and shorter VBC–VBC links for a given DOG (Scheme 5a).

There seems to be also an effect of the base polymer on the stability of the grafted AEM. While this effect is minimal compared to the dose rate effect, it is still significant. At similar grafting conditions (dose rate, DOG, *etc.*), the LDPE-based AEM showed 25% slower degradation rate compared to that of HDPE across the studied dose rates. This might arise from the differences in the structural change, *e.g.* cross-linking, that the base polymer is undergoing under radiation. Since crosslinking takes place between carbon atoms in neighbouring chains or chain branches joining together with other branches of the chain, a highly branched polymer like LDPE is more amenable to crosslinking compared to linear polymer like HDPE.[71] It has been shown that under our radiation dose (maximum of 20 kGy for LDPE/HDPE) *i.e.* below total dose of 100 kGy, LDPE polymer experiences significantly higher cross-linking under radiation than HDPE, with both approaching similar cross-linking values

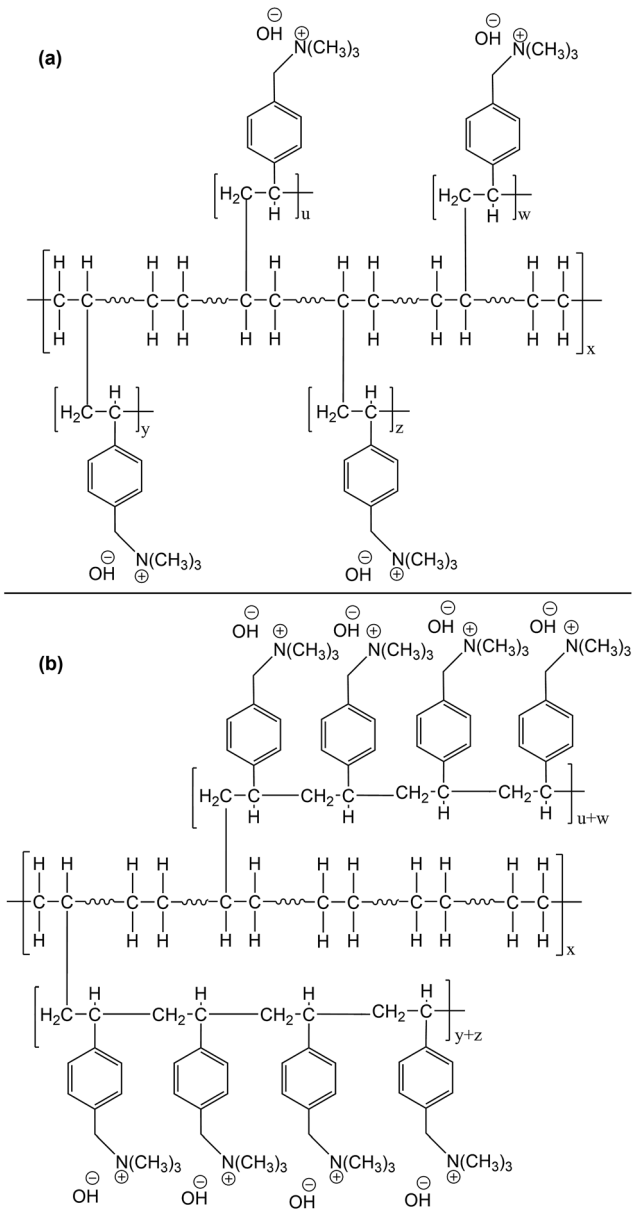

Scheme 5 Possible structures of functionalised AEM after radiation grafting.

at 250 kGy.[72] Additionally, the highly branched LDPE provides more accessible grafting sites in comparison to HDPE (seen by higher DOG for the same grafting conditions) which could translate to better grafting distribution and consequently shorter grafts.

The large variation in grafting requirements of LDPE/HDPE (10–20 kGy) and that of ETFE (70 kGy) makes direct comparison of degradation rate difficult. In the case of ETFE, membrane fabrication using gamma radiation did not produce high enough graft of VBC monomer.[16] ETFE-based membranes were then produced *via* electron beam radiation grafting since high energy electron beam is capable of providing higher dose rate. At a dose rate of 400 Gy h^{-1}, ETFE-based AEM (ET-1 and ET-2) showed IEC loss of 13–15% somewhere in the middle range of IEC loss of LDPE of 21% for 67 Gy h^{-1} (LT-4) and 11% for 2000 Gy h^{-1} (LT-1).

4.3 Effect of functional head group

Fig. 1 shows a comparison in IEC drop between TMA- (LT-1) and DABCO-functionalised (LD-1) membranes both having the same DOG of 65% (2000 Gy h^{-1}). The LT-1 membrane exhibited higher initial IEC than the mono-quaternised LD-1 membrane (as shown later by NMR data) since TMA can more effectively penetrate the LDPE-*g*-VBC copolymer compared to DABCO due to the bulkier structure of DABCO. The lower IEC with the use of DABCO is still acceptable, provided that the resulting membrane is more chemically and thermally stable.[73]

The degradation rates for both membranes were very similar, with IEC loss of 13.0% for DABCO in comparison to 11.1% for TMA. These results were obtained under neutral pH (deionised water) and not in highly alkaline media, where the hydroxide counter ions associated with the head group might not be able to start the nucleophilic attack leading to head group loss under Scheme 1 but rather could undergo ylide formation reaction (Scheme 2). It can be seen that the degradation rate in our tests was less dependent on the head group in comparison to the accelerated tests on the head groups alone in high temperature and alkaline concentration (2 M KOH at 160 °C) which showed much better stability of DABCO than TMA with half-time disintegration of 42 and 29 min, respectively.[40] It also suggests that the degradation mechanism under low alkaline concentration and relatively low temperature of 60 °C might be different from the mechanisms reported under accelerated testing using high alkaline concentrations and temperature using single monomer unit.

4.4 Effect of the temperature and degradation time on the membrane stability

The effect of temperature on the degradation rate was studied where representative samples of AEM with varying base polymers (LDPE and HDPE, 35 Gy h^{-1} and ETFE, 400 Gy h^{-1}; Table 2) were subjected to stability tests employing the same procedure but with increasing temperature and time (Table 3). There was a negligible decrease in IEC at low temperatures of 20 and 40 °C after a 1 month period indicating that the AEMs are stable at temperatures up to 40 °C. At 60 °C, a measurable decrease of IEC was recorded after a 1 month period as discussed earlier.

4.5 Ionic conductivity of the initial and aged membranes

IEC is a measure of the concentration of the functional groups present to transfer the hydroxide ions and a higher IEC consequently results in a higher ionic conductivity. Loss of functional groups due to membrane's degradation results in lowering its IEC and decrease its measured ionic conductivity.

Table 4 shows the through-plane ionic conductivity at 60 °C of HDPE-based membranes, HT-2 and HT-3. Degradation tests on the membranes after 2 months revealed a decrease in ionic conductivity of the membrane (60 °C) by 37.0% (84 to 53 mS cm^{-1}) and 24.7% (101 to 76 mS cm^{-1}). Similarly, LDPE-based membranes showed a decrease in ionic conductivity

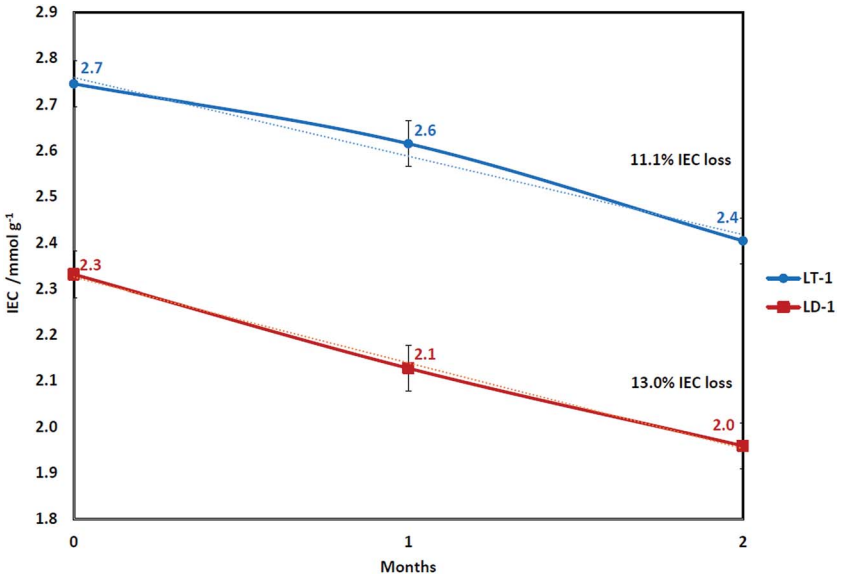

Fig. 1 The IECs of LT-1 and LD-1 membranes after soaking in deionised water at 60 °C.

Table 3 The IECs of membranes in deionised water soaked for different time intervals and temperatures

Membrane	Initial IEC (mmol g^{-1})	IEC month 1 (mmol g^{-1})			IEC month 2 (mmol g^{-1})
		20 °C	40 °C	60 °C	60 °C
LT-3	2.4 ± 0.2	2.3 ± 0.1	2.2 ± 0.1	2.0 ± 0.1	1.6 ± 0.1
HT-2	2.6 ± 0.2	2.5 ± 0.2	2.5 ± 0.2	2.4 ± 0.2	1.4 ± 0.1
ET-2	1.5 ± 0.1	1.5 ± 0.1	1.5 ± 0.1	1.4 ± 0.1	1.3 ± 0.1

Table 4 Through-plane ionic conductivity at 60 °C of AEMs before and after 2 months degradation test

Membrane	Radiation dose rate (Gy h^{-1})	Functionality	Ionic conductivity (mS cm^{-1})	
			Initial	After 2 months
HT-2	35	TMA	84 ± 4	53 ± 3
HT-3	67		101 ± 5	76 ± 4
LT-4	67	TMA	84 ± 4	68 ± 3
LT-1	2000		99 ± 5	85 ± 4
LD-1	2000	DABCO	69 ± 3	52 ± 3

(60 °C) of 19.0% (84 to 68 mS cm^{-1}) and 14.1% (99 to 85 mS cm^{-1}) for LT-4 and LT-1 membranes, respectively. The decrease in ionic conductivity agrees well with the observed decrease in IEC reported in Table 2 and confirms the earlier conclusion that membranes prepared under high radiation dose rate demonstrates slower degradation compared to using low dose rate. Furthermore, it also confirms that the degradation rate using LDPE-based AEM is slower compared to that of HDPE-based AEM using the same grafting conditions.

The LT-1 membrane showed lower decrease in ionic conductivity at 60 °C after 2 months of 14.1% compared to LD-1 membrane, which showed a decrease of 24.6% (using the same radiation dose rate of 2000 Gy h^{-1}). While both AEMs using TMA and DABCO showed the same % IEC loss after 2 months, the bulkier structure of DABCO and its lower basicity (pK_a = 8.72) compared to TMA (pK_a = 9.81) results in lower conductivity at similar DOG and IEC. This translates to a larger activation energy of DABCO-based AEM (E_a = 14 kJ mol^{-1}) for OH^- ion conductivity and consequently larger effect of IEC decrease on conductivity in comparison to TMA-based AEM (E_a = 12 kJ mol^{-1}).[10]

4.6 Scanning electron microscopy analysis

Fig. 2a and b show the scanning electron microscopy (SEM) images of the surface and cross-section, respectively, of the aged LDPE-based membrane prepared under 35 Gy h^{-1} dose rate (LT-3). The observed voids (bubbles) suggest that part of the polymer was lost and dissolved in the surrounding water during the degradation process leaving the void behind. This is most likely to be the grafted vinylbenzyl groups and not simply the functional head group alone.

While polyvinylbenzyl trimethylammonium chloride or hydroxide is water soluble, the grafted LDPE-*g*-VBC-TMA-OH is not and the potential loss of polymer seen by the SEM must be caused by the degradation mechanism as such degradation/loss was not observed with LDPE-*g*-VBC-TMA-Cl (from IEC data, Table 1). It also suggests that at such dose rate, the VBC has relatively longer chains and is less distributed throughout the grafted polymer (for a given DOG). Hence, upon scission of the VBC–VBC link, long chains of water soluble vinylbenzyl trimethylammonium hydroxide are lost leaving the large void space observed behind, it was reported[74] that at low DOG < 11% bubbles on the membrane surface was observed after grafting and functionalisation due to the strong imbalance between

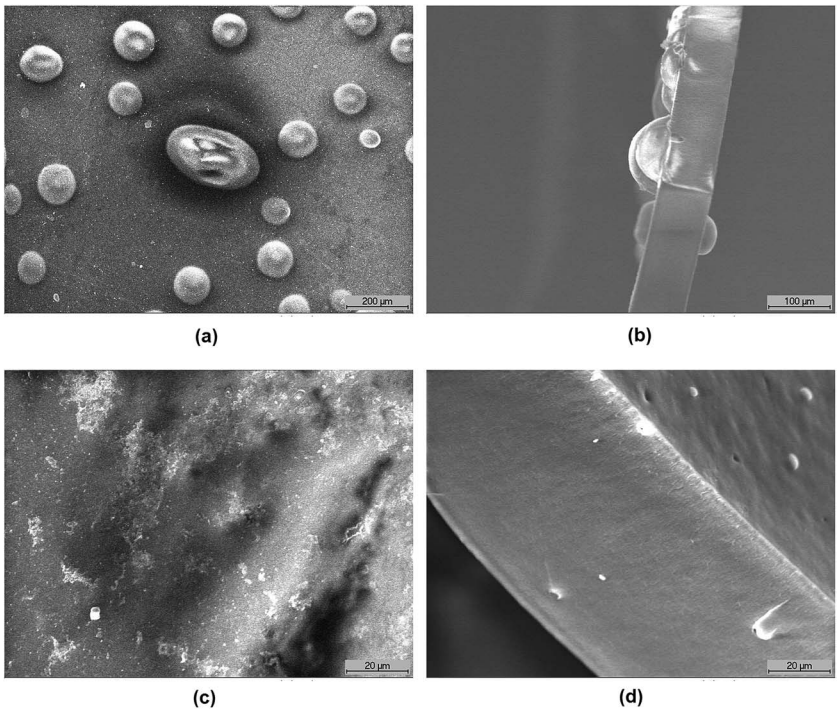

Fig. 2 SEM micrographs of (a) surface at 100× and (b) cross-section at 200× magnification of the aged LT-3 membrane, and (c) surface and (d) cross-section at 1000× magnification of the aged LT-1 membrane.

hydrophobic bulk film and the hydrophilic functionalised layer and the bubbles disappeared at DOG levels above 10%. However, this reported imbalance is inapplicable in this study, the investigated LT-3 and LT-1 AEMs have DOG significantly higher than 10%, namely 58% and 65%, respectively. Moreover, the initial functionalised membranes did not show formation of bubbles. Furthermore, the presence of bubbles were only observed after prolonged degradation test (Fig. 2a and b) and are associated with the loss of IEC.

The image of the cross-section of the aged membrane seems to suggest that the degradation starts on the surface then progresses through the membrane. Fig. 2c and d show the surface and cross-sectional structure, respectively, of the aged LDPE-based AEM prepared under higher radiation dose rate of 2000 Gy h^{-1} (LT-1). SEM micrographs were taken at higher magnification (1000×) and the membranes were still visibly smooth and lacked any bubbles. This supports the earlier results concluding that mutual radiation grafting performed under high dose rate produces more stable AEMs compared to applying low radiation dose rate and suggests that the loss of VBC is more uniform in the structure. This can be explained by better distribution of VBC in the grafted polymer with shorter grafted chains and higher cross-linking resulting in less water soluble by-products. This will be discussed further using various chemical analysis techniques.

4.7 NMR spectroscopy analysis

4.7.1 NMR analysis of the aged membranes and the degradation solution. Solid-state NMR spectroscopy was employed on both the original and the aged TMA- and DABCO-functionalised membranes (in OH^- form stored in deionised water at 60 °C for 2 months) to determine the decrease of various chemical groups present as an initial attempt to identify the decomposition products (Fig. 3 and 4). The ^{13}C CP-MAS NMR peaks were observed to be broad, which is usually expected for polymers, while the intensities of the signals are not normally proportional to the number of equivalent ^{13}C atoms (unlike ^{1}H NMR) and are instead strongly dependent on the number of surrounding spins (typically ^{1}H). This means for example, that the ratio of aromatic ring ^{13}C peaks to that of LDPE ^{13}C is lower than the estimated molar ratio value from the DOG. However, a decrease in that ratio under the same NMR test conditions (relaxation time, *etc.*) suggests a decrease in the aromatic group content. The ^{13}C CP-MAS NMR spectra obtained were normalised against LDPE peaks since the base polymer was not detected in the degradation products.

Comparison of the spectra of the initial and aged membranes revealed a decrease in the intensity ratio of the benzyl group to that of LDPE, which indicates decrease in the amount of the particular group in the membrane structure.[75] Furthermore, no new signals were detected in both ^{13}C and ^{15}N CP-MAS NMR spectra suggesting no degradation by-products has formed on the membrane itself, the degradation products therefore are water soluble and can be identified in the solution.

Fig. 3a shows the ^{13}C CP-MAS NMR spectra of the initial and aged LT-4 membrane. The aromatic ring carbons (benzyl groups) give the resonance between 125 and 150 ppm. The signals between 190 and 220 ppm and the smaller broad signal between 55 and 85 ppm are spinning sidebands associated to the aromatic carbons. The CH–CH_2 groups resonate at 40–50 ppm,

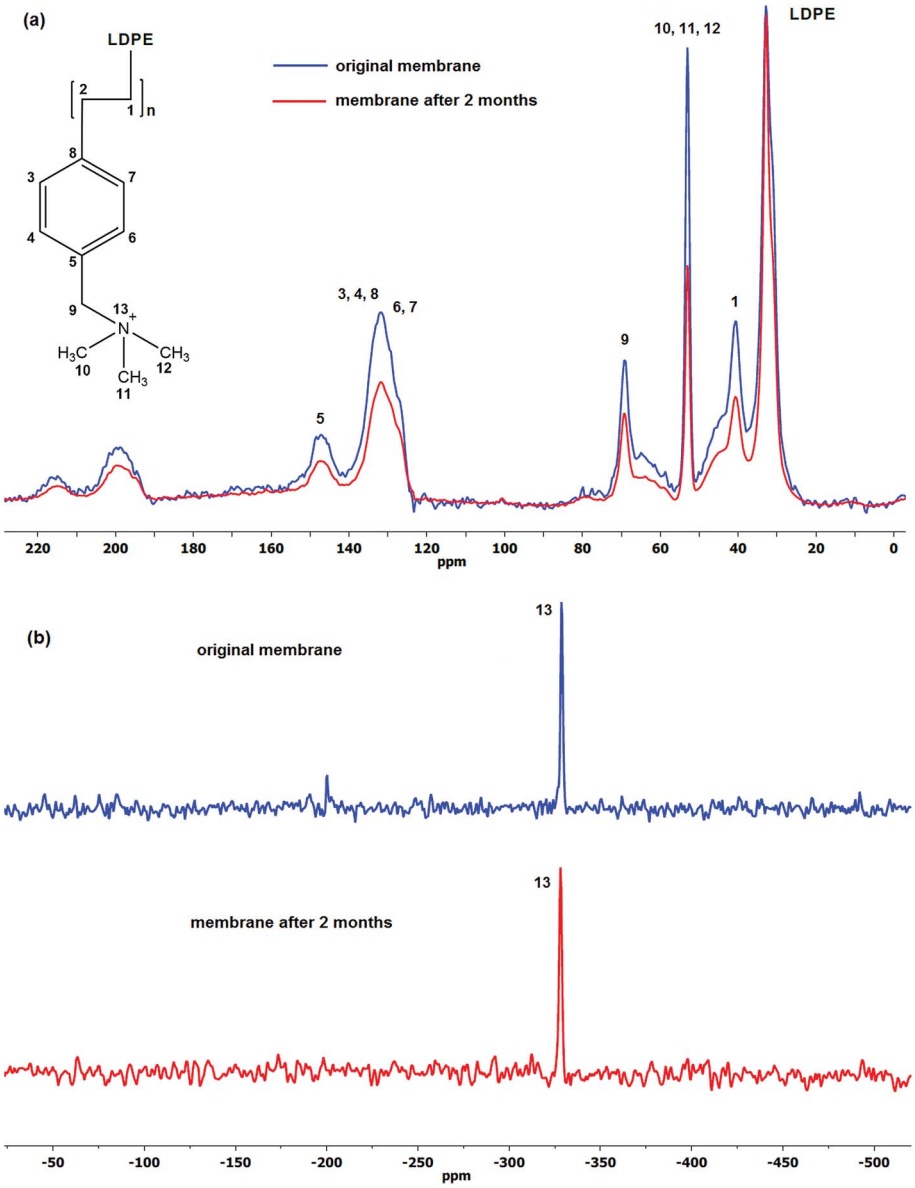

Fig. 3 The (a) ^{13}C and (b) ^{15}N CP-MAS NMR spectra of the original and aged LT-4 membrane.

$N(CH_3)_3$ at 53 ppm and LDPE aliphatic carbons around 20 to 35 ppm. The 69 ppm resonance is assigned to the $-CH_2N$.[76–78]

It is clear from the spectra that there are losses in the VBC and ammonium (TMA) group peak size. The results show 1 : 1 ratio of VBC to TMA loss wherein the percentage of the loss to their initial values after 2 months degradation was *ca.* 30%. This agrees well with the observed loss of IEC of *ca.* 22% and indicates that the majority of the degradation is caused by the loss of the whole vinylbenzyl trimethylammonium hydroxide and not simply just the TMA head group. This is significant since all the proposed mechanisms in the literature involve loss of only the head group (TMA) and not the VBC groups. It was further observed that the ratio of VBC to TMA loss remained close to 1 using high radiation dose rate (2000 Gy h^{-1}, 66% DOG).

Fig. 3b on the other hand, shows the ^{15}N CP-MAS NMR spectra of the same LT-4 AEM. The same quaternised nitrogen peak of TMA at −330 ppm[79] can be seen and no other resonance peaks were observed after degradation suggesting that no other nitrogen-containing by-products have formed on the membrane.

Similarly for the DABCO-functionalised membrane (LD-1), the ^{13}C CP-MAS NMR spectra shown in Fig. 4a share common peaks with that of TMA-based AEM namely, the aliphatic carbon peaks of LDPE at 20 to 35 ppm and the aromatic carbons between 120 to 150 ppm. Total Suppression of Spinning Sidebands (TOSS) was employed during analysis in order to minimise the impact of the spinning sidebands. There are two strong peaks at 46 and 53 ppm representing the carbons attached to the unquaternised and quaternised nitrogen, respectively.[80] It can be seen that the sizes of both of those peaks are very similar suggesting equal amounts of unquaternised and quaternised nitrogen, *i.e.* mono-substituted DABCO which

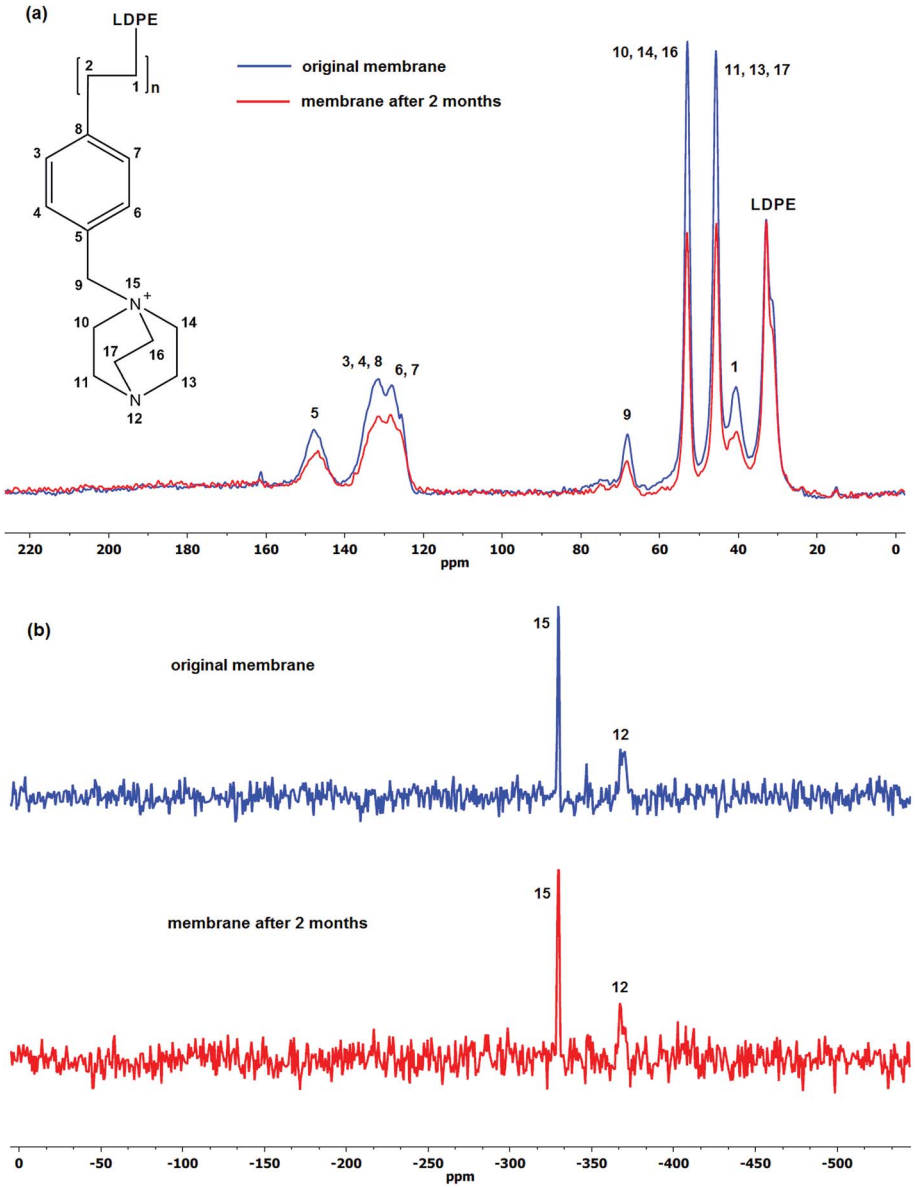

Fig. 4 The (a) ^{13}C and (b) ^{15}N CP-MAS NMR spectra of the original and aged LD-1 membrane.

is supposed to offer better stability over double substitution.[40] After 2 months degradation period, there is a marked decrease in the peak intensity at 40 ppm indicating loss of VBC, similar to what was observed with the LT-4 membrane (Fig. 3a). However, unlike the aged LT-4 membrane, the results indicate VBC to DABCO loss of 1 : 2 ratio with loss to its initial values of *ca.* 15% which is in agreement with the observed IEC loss of 13% (Fig. 1).

The resonance peak at −330 ppm in the ^{15}N CP-MAS NMR spectra shown in Fig. 4b is consistent with the quaternised nitrogen in the DABCO structure and the peak at −368 ppm can be associated with the unquaternised nitrogen, both present in the original and degraded membrane.[81] Furthermore, no other additional resonance peaks were observed. Unfortunately, the peaks in ^{15}N CP-MAS NMR spectra cannot be integrated to quantify the relative loss of DABCO-nitrogen in both original and degraded membranes.

Nuclear magnetic resonance (NMR) has been the most commonly established method of analysing and monitoring degradation of ionomer membranes.[54,82,83] In order to shed more light on the role of OH^- ion and oxygen on the degradation process, both solid-state and solution ^{17}O NMR spectroscopy were utilised in order to determine the presence of possible oxygen-containing compounds which could help elucidate the AEM degradation reactions.[84] The ^{17}O DE-MAS NMR spectra of the aged LT-1 membrane revealed clear identifiable peaks even with a moderate signal-to-noise ratio that suggests oxidation of the aged membrane as shown in Fig. 5a. Similarly, the water–^{17}O solution wherein the isotope-labelled LT-1 membrane had undergone degradation, was subjected to

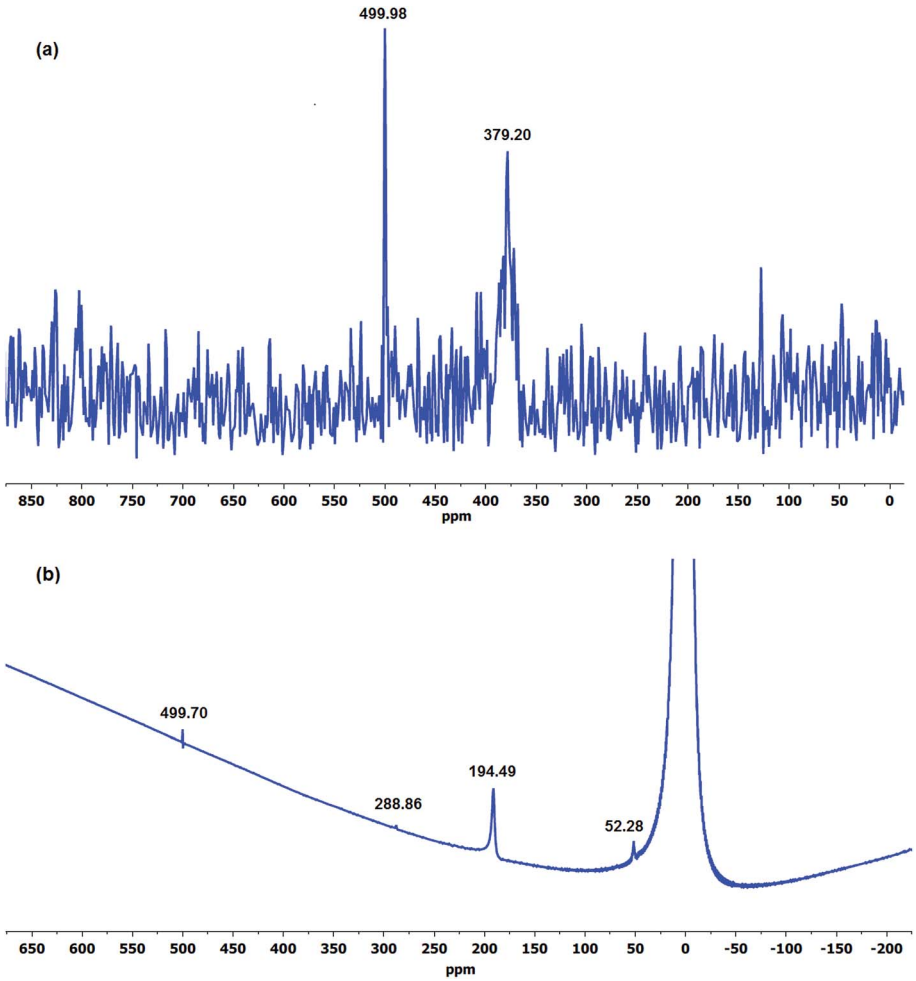

Fig. 5 The ^{17}O (a) DE-MAS NMR spectra of aged LT-1 membrane and (b) solution-NMR spectra of the degradation solution after stability test.

^{17}O solution-NMR (Fig. 5b). As expected, the spectra of the solution appear to show predominantly oxygen from $H_2{}^{17}O$ solvent and alkaline $^{17}OH^-$ ion,[85] but also show other peaks indicating the presence of degradation products.

Experimental data obtained at 120 °C employing Ag_2O-mediated ion exchange reaction have verified mechanism (Scheme 1) indicating formation of a benzylic alcohol and release of TMA as predominant degradation products.[50] However, the presence of a benzylic alcohol cannot be ascertained from the ^{17}O NMR spectra (Fig. 5) since its expected chemical shift (0.7 ppm)[86] is masked by the predominant oxygen resonance of $H_2{}^{17}O$ and ^{17}OH. This can also be due to the possible conversion of benzylic alcohol to dibenzylic ether.[57] Furthermore, the peak at 379 ppm (Fig. 5a) suggests presence of carbonyl-containing (C═O) compounds[87,88] indicating that the benzylic alcohol, if present, is not the final form of the degradation product, but rather could have undergone subsequent oxidation reactions. Considering that the membrane was subjected to a degradation period of 2 months at 60 °C, the benzylic alcohol by-product may have undergone auto-oxidation to produce aromatic aldehydes and/or other carbonyl compounds.[89] Aromatic aldehydes can readily transform to the corresponding carboxylic acid and/or benzylic peroxide radicals.[90] This benzylic peroxide radical could lead to a variety of side reactions, which may cause release of benzyl-TMA group from the membrane. The benzylic peroxide radical could have also been responsible for the oxidation of TMA indicated by the presence of N-oxide (N–O) groups (resonance at 500 ppm)[88] detected on the aged membrane (Fig. 5a) and in the degradation solution (Fig. 5b). In addition, the broad resonance at around 170 ppm in the ^{13}C CP-MAS spectra (Fig. 6) and the FTIR signals at 1057 (□) and 1730 (▲) cm^{-1} of the degradation products (Fig. 8) provide further evidence of the presence of carbonyl-containing compounds indicating that either both the benzylic alcohol and TMA group might underwent subsequent oxidation and such auto-oxidation reactions could have caused the decrease in IEC of the membrane, or other peroxide radicals could have attacked the VBC–TMA group resulting in the observed carbonyl and N-oxide groups.

The presence of degradation products in the solution was attributed to the detected resonance peaks as shown in Fig. 5b. The peak at 194 ppm corresponds to peroxides (O–O) and/or soluble carbonate ($CO_3{}^{2-}$) compounds[91] present in the solution. There are also common peaks observed in both the solution and solid-state ^{17}O NMR spectra, such as the peak at 500 ppm

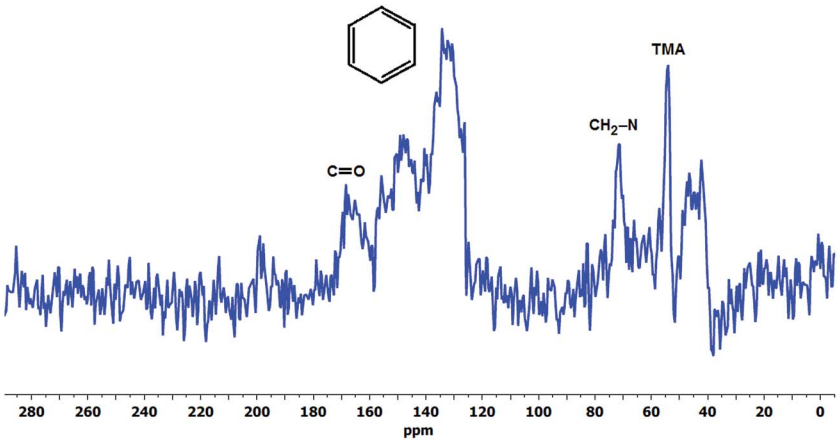

Fig. 6 The ^{13}C CP-MAS NMR spectra of the degradation products of LT-1 membrane recovered after drying the degradation solution.

indicative of oxidised TMA group (N-oxides) and the resonance at 52 ppm (–OH and –O– group)[92] suggesting the presence of similar functional groups in both the degradation solution and the aged membrane. However, further studies are required to identify all of the oxygen-containing products observed.

4.7.2 NMR analysis of the solid degradation products. Fig. 6 and 7a show the ^{13}C CP-MAS NMR spectra of the solid degradation products for both LT-1 and LD-1 membranes after the stability test, respectively. The characteristic resonance of the aliphatic carbons of the base polymer between the 20 to 35 ppm range for the degradation products for both TMA- and DABCO-functionalised membranes is clearly absent, proving that the LDPE is not part of the degradation products. The strong peak at 53 ppm corresponding to the methyl groups in TMA and the resonance peaks within the 130 to 160 ppm region attributed to aromatic ring carbons are both present in the degradation product of the LT-1 membrane (Fig. 6). Furthermore, the peak at 69 ppm (CH_2–N) indicates that the benzyl-TMA groups were detached as a whole from the polymer backbone which is consistent with the observed 1 : 1 ratio of VBC to TMA loss between the original and aged membrane (Fig. 3). Such loss of benzyl-TMA groups can explain the observed decrease in IEC and the large voids seen in SEM (Fig. 2). This is in contrast with typically suggested elimination degradation mechanism which produces only TMA and/or methanol as proposed by-products.[19,25] It should be stressed that the later mechanisms are typically suggested in high alkaline media. The broad resonance in the 170 ppm region indicates the presence of carbonyl groups (C=O) suggesting formation of oxidative degradation products discussed earlier. Unfortunately, an attempt to obtain a ^{15}N CP-MAS NMR spectra for the degradation product of the LT-1 membrane was unsuccessful due to low absolute intensity of the carbon spectrum.

Unlike TMA, some of the DABCO upon detachment from the membrane was observed to recrystallise from the solution upon cooling to room temperature. DABCO was subsequently separated by centrifuge and was present predominantly in mono-quaternised form as indicated by the two strong carbon peaks at 45 and 53 ppm as shown in Fig. 7a. Furthermore, the resonance at −330 ppm attributed to quaternised nitrogen in the ^{15}N CP-MAS NMR spectra (Fig. 7b) suggests the detachment of benzyl trimethylammonium groups. The intense resonance of DABCO indicates its presence in excess than VBC in the degradation product which is in agreement with the 1 : 2 ratio of VBC to DABCO loss as observed in Fig. 4a. Since the prepared LD-1 AEM is largely mono-quaternised (weak −368 ppm resonance, Fig. 4b), the unquaternised nitrogen is expectedly too weak to be detected in the degradation products (Fig. 7b).

4.8 FTIR analysis of the solid degradation products

Fig. 8 shows the FTIR spectra of the degradation products (residue isolated from the solution) of TMA-functionalised membrane having different base polymers. It was very evident in all spectra of the degradation products (deg prdt) that there were no detectable strong peaks between the 2800 and 3000 cm^{-1} region. The 2850 (‡) and 2920 (†) cm^{-1} peaks in the spectra of the initial membranes are attributed to the $-CH_2$ symmetric and asymmetric stretching, respectively, both of which are characteristic peaks of the ETFE (ET-2), LDPE (LT-1) and HDPE (HT-3).[93–95] Additionally for the ET-2 degradation product, there is a clear absence of intense peaks between 1000 and 1300 cm^{-1} (§) region that can be associated with C–F stretching vibrations.[96,97] This agrees with the NMR analysis (Fig. 6) wherein the absence of these characteristic peaks indicates that the base polymers were thermally stable and did not degrade as they were not detected in the degradation products.

Fig. 8 clearly shows that the spectra of the degradation products for all the different base polymers are identical. This indicates that same degradation products were recovered after the stability test regardless of the type of polymer backbone used. The precipitate contains VBC groups evinced by bands observed at 840 (●) and 700 (♦) cm^{-1} which are consistent with the *meta* and/or *para* benzene ring substitution.[98] The presence of TMA is attributed to the C–N stretch at 880 cm^{-1} (♣) and the N–CH_3 symmetric bending deformation at 1393 cm^{-1} (△)[99] while the band at 1440 cm^{-1} (■) refers to the $-CH_2$ scissoring vibrations.[100] The peak at 1660 cm^{-1} (○) is due to the O–H

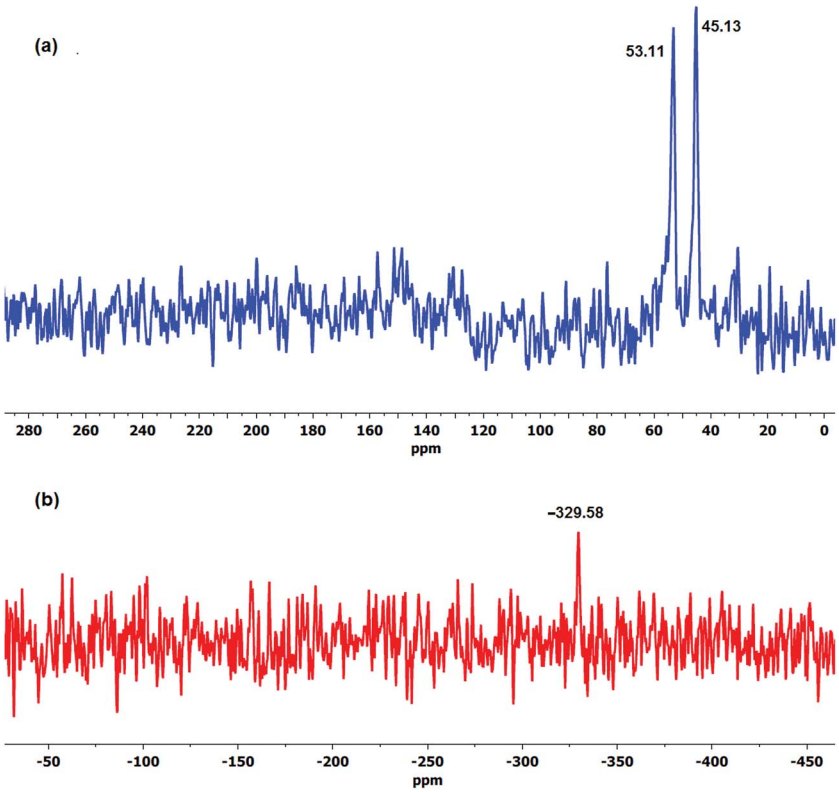

Fig. 7 The (a) ^{13}C and (b) ^{15}N CP-MAS NMR spectra of the degradation products of LD-1 membrane after stability test.

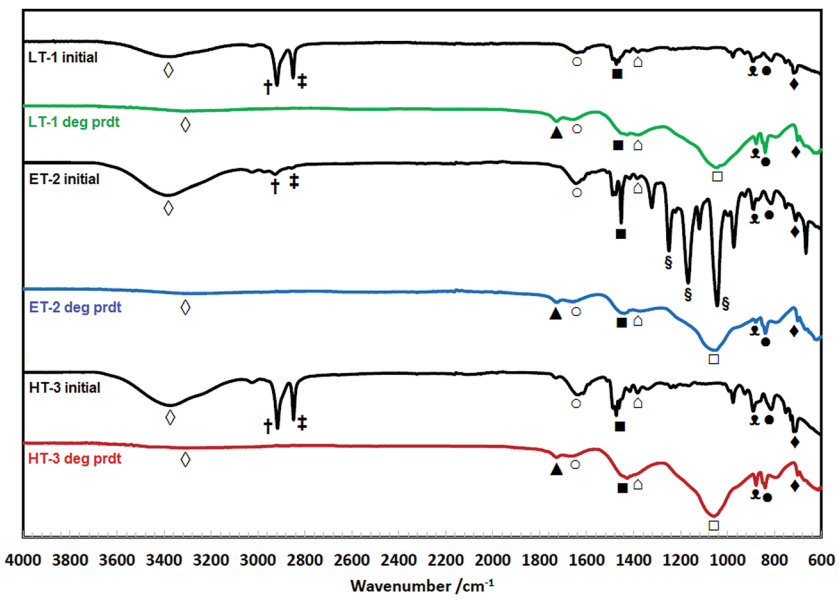

Fig. 8 FTIR spectra of the initial TMA-functionalised membranes and the degradation products (deg prdt) with different polymer backbones.

bending of hydrogen bonded water associated with tetramethylammonium hydroxide (TMAH) hydrate.[101] This is different with the weak signal observed between 3300 and 3400 cm^{-1} (◊) region that is associated with O–H stretching due to possible presence of residual water and/or OH in the degradation product.

The possible presence of carbonyl-containing compounds in the degradation products is shown by the strong C–O and C=O stretching vibrations at 1057 (□) and 1730 (▲) cm^{-1}, respectively.[102]

The FTIR spectra of the degradation product from the LDPE-based membrane functionalised with DABCO (LD-1) is shown in

Fig. 9. Similar to the TMA-functionalised membrane (Fig. 8), there is no detected presence of LDPE base polymer in the degradation products as there were no strong peaks observed between the 2800 and 3000 cm^{-1} region, which also confirms with the NMR analysis (Fig. 7). The peaks observed at 1700 (▲), 1057 (□) and 583 cm^{-1} (ϑ) suggest existence of carbonyl-containing (aldehyde and/or ketone) by-products, while the bands at 848 (●) and 796 cm^{-1} (Δ) are attributed to the *meta* and/or *para* substitutions of the VBC[98] indicating presence of aromatic compounds in the degradation product. The presence of DABCO in the degradation product was confirmed by the bending deformation at 1460 cm^{-1} (■) of the CH_2 groups[103] while the strong signal at 1030 cm^{-1} (✱) is due to C–N stretching vibrations in the DABCO structure.[104,105]

4.9 Mechanism of AEM degradation

Studies on the mechanisms of degradation and measurements of the degradation rates of fabricated membranes reported in the literature were all performed in media with high alkaline concentration and temperature. The degradation rates reported therein are driven predominantly by the loss of head group due to very high alkaline concentration (OH^- ion attack) at elevated temperature (Scheme 1). However, such test conditions are actually very far from the real operating environments of low-temperature fuel cells and electrolysers (*i.e.* close to neutral medium). As previously discussed, AEM degradation due to IEC loss was observed even at very low alkaline concentration (deionised water) at temperature of 60 °C. Results suggest that not only the loss of TMA head group and VBC monomer were responsible for the loss of IEC but also parallel oxidation processes are likely taking place that provide other routes to degradation. Therefore, in actual fuel cell and electrolyser systems that use water media with very low alkalinity and constantly exposed to oxygen gas, the investigation of membrane degradation should shift to the effect of varying the oxygen concentration rather than simply the OH^- ion concentration on stability. Consequently, this suggests that the rate of membrane degradation due to auto-oxidation can have a significant impact aside from the established degradation mechanisms due to loss of head group.

The decrease in ionic conductivity brought about by the decrease in IEC due to the degradation of the fabricated membrane is more pronounced under 100% humidified stream of oxygen than nitrogen at 80 °C as we have reported previously.[41] The degradation rate in terms of ionic conductivity is 4 times faster in oxygen than in nitrogen which suggests that at very low alkaline concentration, such four-fold increase in degradation rate indicates another degradation mechanism taking place alongside (*i.e.* oxidation) or at very low alkaline concentration with negligible head group loss (Scheme 1) one mechanism that is accelerated by oxygen concentration.

The observed *ca.* 5.5% loss after 1 month in air-saturated deionised water at 60 °C (Fig. 1, LT-1) was compared with reported degradation rates in literature. Einsla *et al.*[55] observed a 10% loss of benzyltrimethylammonium (BTMA) cation (compound) at 80 °C after 1 month under 1 M alkaline and nitrogen atmosphere. There was no change in degradation rate in the studied alkaline concentration range between 1–5 M. Using the reported activation energy (15.8 kcal mol^{-1}), the degradation rate at 60 °C of the same BTMA cation was estimated to be 2.6% after 1 month in 1 M KOH. This is less than half of the % loss after 1 month in air-saturated deionised water we obtained of 5.5% with the highest radiation dose and an order of magnitude lower than the lowest dose rate (25%) indicating that the degradation of the fabricated membranes investigated is not only due to the removal of the head group but could also due to other mechanisms involving oxygen.

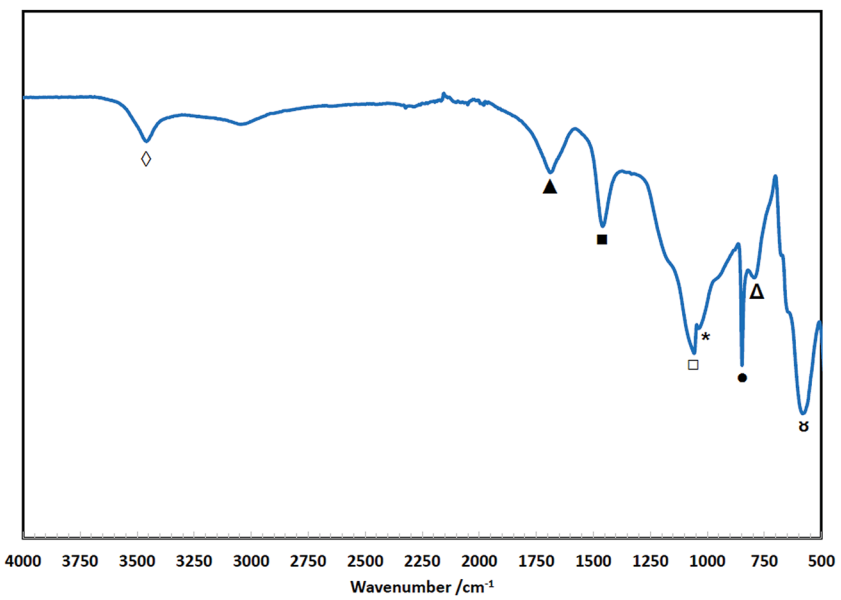

Fig. 9 FTIR spectra of the degradation products of LD-1 membrane.

We therefore suggest an alternative degradation mechanism for AEMs immersed in close to neutral pH solutions (deionised water) that involves oxidation of the initial degradation products and the ylide intermediate (Scheme 6) which can explain the above observations. A parallel observation that suggests peroxide radicals could be generated from ylide (Scheme 2) was recently reported[33] employing ^{31}P NMR spectroscopy and using polyphenylene oxide (PPO) as base polymer for the TMA-based AEM. It was reported that auto-oxidation is favoured under alkaline conditions and the degradation of AEM was due to hydroxyl and superoxide anion radicals formation which were found to be responsible for the PPO backbone chain scission.

In the proposed mechanism (Scheme 6), the degradation of the membrane is governed by 2 reaction routes (A and B) which can proceed simultaneously. Initially, in alkaline environment, AEM degradation proceeds with the loss of the head group (Scheme 1) as widely reported, hereby indicated as Reaction A. The reaction rate (r_1) in terms of loss of head group is a function of the OH^- ion concentration and operating temperature, wherein subjecting the membrane to highly alkaline media and temperature expect a high degradation rate *via* head group loss. The initial degradation products of Reaction A could subsequently undergo auto-oxidation/oxidation to form benzylic peroxide radicals and TMA-oxide radicals. The reaction rate in terms of auto-oxidation reaction is dependent on temperature and on degradation products and oxygen concentrations, wherein as more oxygen is fed to the system at constant alkaline concentration and temperature, more N-oxide and peroxide radicals will be created. These benzylic peroxide radicals and TMA-oxide radicals could possibly attack the benzylic carbon liberating VBC–TMA causing further decrease in IEC of the AEM depending on the length of the VBC grafts, *n*. However, we

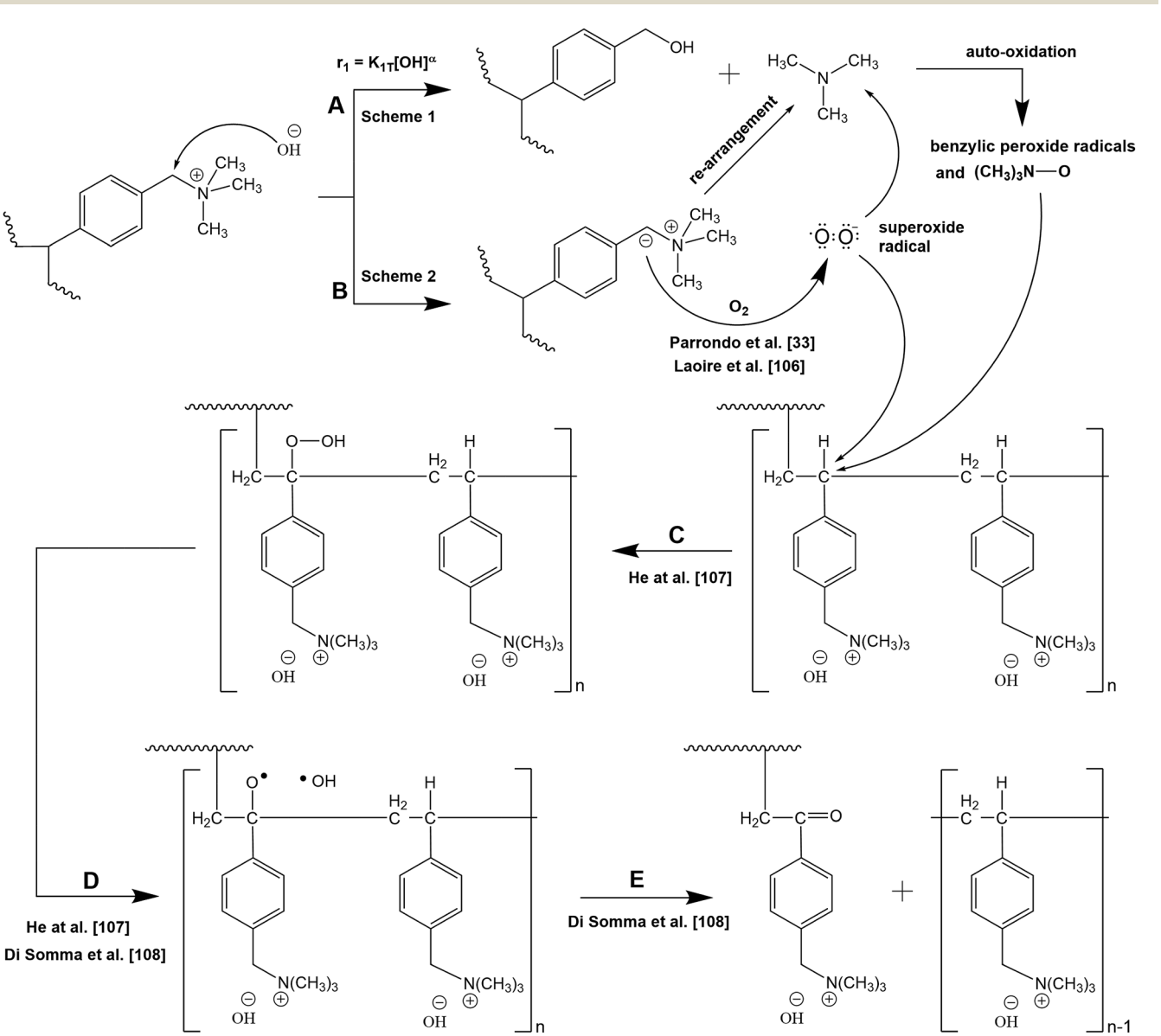

Scheme 6 Proposed degradation pathways for TMA-functionalised AEM in media with very low alkaline concentration.

observed 1 : 1 ratio of VBC to TMA loss of prepared LT-4 AEM (Fig. 3), suggesting that at very low alkaline concentration, the loss of head group due to OH^- ion attack (Reaction A) has minor contribution to membrane degradation and is rather mainly attributed to the loss of VBC–TMA group as a whole (Reaction B).

The degradation route *via* Reaction A can be applicable to DABCO-based AEM (LD-1) where a 1 : 2 ratio of VBC to DABCO loss was observed (Fig. 4) indicating better stability of TMA than DABCO even at same radiation dose rate due to more loss of DABCO head group than VBC. This suggests that the degradation of LD-1 membrane is not solely due to removal of the whole VBC–DABCO group but could also involve the auto-oxidation of the initial degradation products of the nucleophilic substitution reaction (*i.e.* membrane degradation proceeds through both Reaction A and B). Therefore, this indicates that at very low alkaline concentration, the ratio of VBC to head group loss dictates the relative yields of degradation routes and that different head group types could follow one or more degradation pathways depending on the applied radiation dose rate.

Reaction B proceeds as proposed by Parrondo *et al.*[33] wherein the carbanion reduces the dissolved oxygen present in the solution to produce superoxide radicals. Such process involves one-electron reduction of the dissolved oxygen leading to the formation of O_2/O_2^- (superoxide) redox couple.[106] The ylide formation and consequently the superoxide explain why degradation in terms of IEC loss is not due to direct oxygen reaction with VBC–TMA as IEC loss was only observed when the membranes were in the OH^- form and was not observed in Cl^- form (Table 1). The presence of carbonyl-containing compounds and N-oxide groups (Fig. 5) also support the hypothesis of the formation of these superoxides. Consequently, in the absence of high OH^- ion concentration in the surrounding media, these superoxide radicals can attack the vulnerable benzylic carbon of the LDPE–VBC resulting in the release of VBC–TMA groups.

The attack of free radicals (benzylic peroxide, TMA-oxide, or superoxide radicals) on the vulnerable carbon (carbon in *para* position with respect to the trimethyl ammonium hydroxide group) gives rise to the formation of a hydroperoxide moiety (Reaction C) reported for cumene.[107] The hydroperoxide group is expectedly unstable and is easily fragmented to hydroxyl and oxide radicals upon thermal decomposition (Reaction D),[107,108] which subsequently rearranges to form ketone (C=O) by-product and cause the detachment of VBC–TMA chains.[108]

The reaction rate in terms of free radical attack is influenced by the applied radiation dose rate. Therefore, at a fixed operating temperature with constant OH^- ion and oxygen concentration, the degradation rate is solely dependent on the applied radiation dose rate during AEM synthesis. Membranes prepared under low radiation dose rate produce longer VBC–VBC chains (high value of n) resulting in higher IEC loss upon chain scission of the long VBC grafts. As observed in the SEM image (Fig. 2), the even distribution of bubbles (voids) suggests long VBC–VBC grafts as few active sites for LDPE–VBC were created due to low applied radiation dose rate. On the other hand, membranes prepared under high radiation dose rate will have more uniform VBC monomer distribution producing more LDPE–VBC grafts and shorter VBC–VBC links (low value of n), hence slower degradation due to lower IEC loss per attack.

5. Conclusion

The chemical and thermal stability of radiation-grafted anion-exchange membrane (AEM) are important properties that dictate its service life for fuel cell and electrolyser applications. This research has investigated the stability of fabricated AEMs in deionised water which is the usual medium for electrolyser and fuel cell operation. After the stability test, there was an observed decrease in IEC, hence a decrease in ionic conductivity, which is an indication of AEM degradation. The stability of the membrane was found to be influenced by the applied gamma radiation dose rate. The use of higher radiation dose rate produces membranes with enhanced stability due to the improved VBC monomer distribution throughout the grafted monomer, hence more LDPE–VBC grafts and shorter VBC–VBC links. The increase in applied radiation dose rate from 30 to 67 Gy h^{-1} (total radiation dose of 10 kGy) for the LDPE-based AEM significantly reduced the % IEC loss from 37 to 21%, respectively. The same was observed with HDPE-based AEM where the % IEC loss decreased from 50% to 28% with similar increase in radiation dose rate. The stability of the LDPE-based AEM even further improved when the applied radiation dose rate and total radiation dose were increased to 2000 Gy h^{-1} and 20 kGy, respectively, with only 11% IEC loss. The ETFE-based AEMs, on the other hand, were fabricated using an electron beam radiation source and at 400 Gy h^{-1} radiation dose rate demonstrated comparable stability to that of the LDPE based AEM (2000 Gy h^{-1}) having 13–15% IEC loss.

The use of different base polymer types among those investigated revealed minimal effect on the stability of the resulting AEM, which is mainly influenced by the structural changes (*e.g.* cross-linking, chain graft lengths, DOG) during radiation grafting. In terms of functional groups, there was limited effect of the studied head group on IEC% loss, the TMA has emerged to offer slightly better stability than DABCO (under the same radiation dose rate).

NMR (solution and solid-state) and FTIR analyses of both the aged TMA- and DABCO-functionalised membranes and their degradation products confirmed loss of not only the functional group but also the VBC which is in contrast with typically reported degradation mechanisms of AEMs in high alkaline media where degradation is carried out under inert atmosphere using simple BTMA compound instead of polymer membrane. At very low alkaline concentration, the reaction rates of membrane degradation were dependent on both oxygen concentration present in the surrounding media and on the applied radiation dose rate. When the concentration of dissolved oxygen in the solution is increased, the rate of membrane degradation due to IEC loss is also increased, the most likely reason for this is formation of superoxide radicals that attack the vulnerable benzylic carbon and cause the release of VBC–TMA. Moreover, ^{17}O NMR analysis of the aged membrane and the degradation products suggest the presence of carbonyl-containing compounds and N–O compounds indicating that

oxidative processes could possibly take place. Either the benzylic alcohol and TMA by-products are not the terminal form of the degradation products and could undergo further auto-oxidation leading to further loss of VBC through benzylic peroxide radicals attack and TMA-oxide radicals attack, or another more probable explanation is that peroxide radicals generated from dissolved oxygen through the ylide formation are responsible for these oxidations and for VBC–TMA loss. This explains the faster degradation rate under oxygen gas feed compared to nitrogen under fuel cell operation reported previously.[41]

This study therefore recommends that future research on AEM materials and degradation study should be conducted at pH closer to neutral and in oxygen saturated environment. The effort should be on improving AEM stability towards oxidation instead of testing head group stability for E2 or SN2 attack in nitrogen saturated high alkaline environment. Lastly, polymer grafting performed under low radiation dose rate produces long chain grafts that leave large void spaces upon chain scission. Preparation of AEMs with high radiation dose rate resulted in a lower % IEC loss and improved stability explained by shorter grafts length, which the established degradation mechanisms reported in literature have not taken into account.

Acknowledgements

The authors acknowledge the support of the Engineering and Physical Sciences Research Council (EPSRC) for funding under Grant Number EP/M005895/1 and the Philippine Department of Science and Technology through the Engineering Research and Development for Technology Program (ERDT-DOST) for funding Richard Espiritu's PhD fellowship. In compliance with EPSRC rules, data supporting this publication is openly available under an 'Open Data Commons Open Database License'. The additional metadata are available at http://dx.doi.org/10.17634/138124-1. Please contact Newcastle University Research Data Service at rdm@ncl.ac.uk for access instructions. The authors further express their gratitude to the EPSRC National Solid-state NMR Service at Durham University for the solid-state NMR spectra.

References

1 L. Carrette, K. A. Friedrich and U. Stimming, *ChemPhysChem*, 2000, **1**, 162–193.
2 M. Mamlouk, K. Scott, J. A. Horsfall and C. Williams, *Int. J. Hydrogen Energy*, 2011, **36**, 7191–7198.
3 M. Mamlouk, S. M. S. Kumar, P. Gouerec and K. Scott, *J. Power Sources*, 2011, **196**, 7594–7600.
4 M. Mamlouk, X. Wang, K. Scott, J. A. Horsfall and C. Williams, *Proc. Inst. Mech. Eng., Part A*, 2011, **225**, 152–160.
5 C. C. Pavel, F. Cecconi, C. Emiliani, S. Santiccioli, A. Scaffidi, S. Catanorchi and M. Comotti, *Angew. Chem., Int. Ed.*, 2014, **53**, 1378–1381.
6 J. R. Varcoe and R. C. T. Slade, *Fuel Cells*, 2005, **5**, 187–200.
7 Y.-C. Cao, X. Wang and K. Scott, *J. Power Sources*, 2012, **201**, 226–230.
8 E. Antolini and E. R. Gonzalez, *J. Power Sources*, 2010, **195**, 3431–3450.
9 J. R. Varcoe, M. Beillard, D. M. Halepoto, J. P. Kizewski, S. Poynton and R. C. T. Slade, *ECS Trans.*, 2008, **16**, 1819–1834.
10 M. Mamlouk and K. Scott, *J. Power Sources*, 2012, **211**, 140–146.
11 T. Zhou, R. Shao, S. Chen, X. He, J. Qiao and J. Zhang, *J. Power Sources*, 2015, **293**, 946–975.
12 S. Gu, J. Wang, B. Zhang, R. B. Kaspar and Y. Yan, in *Materials for Low-Temperature Fuel Cells*, Wiley-VCH Verlag GmbH & Co. KGaA, 2014, pp. 125–144, DOI: 10.1002/9783527644308.ch06.
13 O. I. Deavin, S. Murphy, A. L. Ong, S. D. Poynton, R. Zeng, H. Herman and J. R. Varcoe, *Energy Environ. Sci.*, 2012, **5**, 8584–8597.
14 T. Sata, M. Tsujimoto, T. Yamaguchi and K. Matsusaki, *J. Membr. Sci.*, 1996, **112**, 161–170.
15 K. Scott, M. Mamlouk, R. Espiritu and X. Wu, *ECS Trans.*, 2013, **58**, 1903–1906.
16 M. Mamlouk, J. A. Horsfall, C. Williams and K. Scott, *Int. J. Hydrogen Energy*, 2012, **37**, 11912–11920.
17 S. Chempath, J. M. Boncella, L. R. Pratt, N. Henson and B. S. Pivovar, *J. Phys. Chem. C*, 2010, **114**, 11977–11983.
18 A. C. Cope and A. S. Mehta, *J. Am. Chem. Soc.*, 1963, **85**, 1949–1952.
19 J. R. Varcoe, P. Atanassov, D. R. Dekel, A. M. Herring, M. A. Hickner, P. A. Kohl, A. R. Kucernak, W. E. Mustain, K. Nijmeijer, K. Scott, T. Xu and L. Zhuang, *Energy Environ. Sci.*, 2014, **7**, 3135–3191.
20 G. Merle, M. Wessling and K. Nijmeijer, *J. Membr. Sci.*, 2011, **377**, 1–35.
21 J. Cheng, G. He and F. Zhang, *Int. J. Hydrogen Energy*, 2015, **40**, 7348–7360.
22 C. Fujimoto, D.-S. Kim, M. Hibbs, D. Wrobleski and Y. S. Kim, *J. Membr. Sci.*, 2012, **423–424**, 438–449.
23 Y. Yuesheng and A. E. Yossef, in *Polymers for Energy Storage and Delivery: Polyelectrolytes for Batteries and Fuel Cells*, American Chemical Society, 2012, vol. 1096, ch. 14, pp. 233–251.
24 C. Vogel and J. Meier-Haack, *Desalination*, 2014, **342**, 156–174.
25 S. Chempath, B. R. Einsla, L. R. Pratt, C. S. Macomber, J. M. Boncella, J. A. Rau and B. S. Pivovar, *J. Phys. Chem. C*, 2008, **112**, 3179–3182.
26 H. Long, K. Kim and B. S. Pivovar, *J. Phys. Chem. C*, 2012, **116**, 9419–9426.
27 C. G. Arges and V. K. Ramani, *ECS Trans.*, 2013, **50**, 2183–2197.
28 G. Ghigo, S. Cagnina, A. Maranzana and G. Tonachini, *J. Org. Chem.*, 2010, **75**, 3608–3617.
29 Z. Wang, in *Comprehensive Organic Name Reactions and Reagents*, John Wiley & Sons, Inc., 2010, DOI: 10.1002/9780470638859.conrr591.

30 G. Couture, A. Alaaeddine, F. Boschet and B. Ameduri, *Prog. Polym. Sci.*, 2011, **36**, 1521–1557.
31 S. J. Peighambardoust, S. Rowshanzamir and M. Amjadi, *Int. J. Hydrogen Energy*, 2010, **35**, 9349–9384.
32 S. A. Nuñez and M. A. Hickner, *ACS Macro Lett.*, 2012, **2**, 49–52.
33 J. Parrondo, Z. Wang, M.-S. J. Jung and V. Ramani, *Phys. Chem. Chem. Phys.*, 2016, **18**, 19705–19712.
34 C. G. Arges and V. Ramani, *Proc. Natl. Acad. Sci. U. S. A.*, 2013, **110**, 2490–2495.
35 K. S. Ngai, S. Ramesh, K. Ramesh and J. C. Juan, *Ionics*, 2016, **22**, 1259–1279.
36 T. N. Danks, R. C. T. Slade and J. R. Varcoe, *J. Mater. Chem.*, 2002, **12**, 3371–3373.
37 Q. Zhang, Q. Zhang, J. Wang, S. Zhang and S. Li, *Polymer*, 2010, **51**, 5407–5416.
38 K. Matsui, E. Tobita, K. Sugimoto, K. Kondo, T. Seita and A. Akimoto, *J. Appl. Polym. Sci.*, 1986, **32**, 4137–4143.
39 S. Gu, R. Cai, T. Luo, Z. Chen, M. Sun, Y. Liu, G. He and Y. Yan, *Angew. Chem., Int. Ed.*, 2009, **48**, 6499–6502.
40 B. Bauer, H. Strathmann and F. Effenberger, *Desalination*, 1990, **79**, 125–144.
41 R. Espiritu, M. Mamlouk and K. Scott, *Int. J. Hydrogen Energy*, 2016, **41**, 1120–1133.
42 Y. Zhang, J. Fang, Y. Wu, H. Xu, X. Chi, W. Li, Y. Yang, G. Yan and Y. Zhuang, *J. Colloid Interface Sci.*, 2012, **381**, 59–66.
43 T. A. Sherazi, J. Yong Sohn, Y. Moo Lee and M. D. Guiver, *J. Membr. Sci.*, 2013, **441**, 148–157.
44 H. Zarrin, J. Wu, M. Fowler and Z. Chen, *J. Membr. Sci.*, 2012, **394–395**, 193–201.
45 N. Li, M. D. Guiver and W. H. Binder, *ChemSusChem*, 2013, **6**, 1376–1383.
46 K. J. T. Noonan, K. M. Hugar, H. A. Kostalik, E. B. Lobkovsky, H. D. Abruña and G. W. Coates, *J. Am. Chem. Soc.*, 2012, **134**, 18161–18164.
47 E. N. Komkova, D. F. Stamatialis, H. Strathmann and M. Wessling, *J. Membr. Sci.*, 2004, **244**, 25–34.
48 H. Xu, J. Fang, M. Guo, X. Lu, X. Wei and S. Tu, *J. Membr. Sci.*, 2010, **354**, 206–211.
49 S. Maurya, S.-H. Shin, M.-K. Kim, S.-H. Yun and S.-H. Moon, *J. Membr. Sci.*, 2013, **443**, 28–35.
50 A. D. Mohanty and C. Bae, *J. Mater. Chem. A*, 2014, **2**, 17314–17320.
51 C. G. Arges and V. Ramani, *J. Electrochem. Soc.*, 2013, **160**, F1006–F1021.
52 H. W. Zhang, D. Z. Chen, Y. Xianze and S. B. Yin, *Fuel Cells*, 2015, **15**, 761–780.
53 J. B. Edson, C. S. Macomber, B. S. Pivovar and J. M. Boncella, *J. Membr. Sci.*, 2012, **399–400**, 49–59.
54 M. R. Sturgeon, C. S. Macomber, C. Engtrakul, H. Long and B. S. Pivovar, *J. Electrochem. Soc.*, 2015, **162**, F366–F372.
55 B. R. Einsla, S. Chempath, L. Pratt, J. Boncella, J. Rau, C. Macomber and B. Pivovar, *ECS Trans.*, 2007, **11**, 1173–1180.
56 T. S. Stevens, E. M. Creighton, A. B. Gordon and M. MacNicol, *J. Chem. Soc.*, 1928, 3193–3197, DOI: 10.1039/JR9280003193.
57 W. K. Musker, *J. Am. Chem. Soc.*, 1964, **86**, 960–961.
58 Z. Yang, J. Ran, B. Wu, L. Wu and T. Xu, *Curr. Opin. Chem. Eng.*, 2016, **12**, 22–30.
59 S. W. Kantor and C. R. Hauser, *J. Am. Chem. Soc.*, 1951, **73**, 4122–4131.
60 A. Singh, *Radiat. Phys. Chem.*, 1999, **56**, 375–380.
61 K. Wündrich, *Radiat. Phys. Chem.*, 1984, **24**, 503–510.
62 S. S. Cota, V. Vasconcelos, M. Senne Jr, L. L. Carvalho, D. B. Rezende and R. F. Côrrea, *Braz. J. Chem. Eng.*, 2007, **24**, 259–265.
63 D. Gheysari, A. Behjat and M. Haji-Saeid, *Eur. Polym. J.*, 2001, **37**, 295–302.
64 K. Yoko, in *Irradiation of Food and Packaging*, American Chemical Society, 2004, vol. 875, ch. 16, pp. 262–276.
65 V. J. Krasnansky, B. G. Achhammer and M. S. Parker, *Polym. Eng. Sci.*, 1961, **1**, 133–138.
66 D. Plester, in *Industrial Sterilization*, ed. P. Briggs and W. Miller, Duke University Press, Durham, NC, 1973, pp. 141–152.
67 K. J. Hemmerich, *Med. Device Diagn. Ind.*, 2000, **22**, 78–89.
68 H. C. Sutton and J. Rotblat, *Nature*, 1957, **180**, 1332–1333.
69 E. Moura, E. S. R. Somessari, C. G. Silveira, H. A. Paes, C. A. Souza, W. Fernandes, J. E. Manzoli and A. B. C. Geraldo, *Radiat. Phys. Chem.*, 2011, **80**, 175–181.
70 M. M. Nasef, H. Saidi, A. M. Dessouki and E. M. Ei-Nesr, *Polym. Int.*, 2000, **49**, 399–406.
71 S. M. Tamboli, S. T. Mhaske and D. D. Kale, *Indian J. Chem. Technol.*, 2004, **11**, 853–864.
72 D. Gheysari and A. Behjat, *Eur. Polym. J.*, 2001, **37**, 2011–2016.
73 M. R. Hibbs, *J. Polym. Sci., Part B: Polym. Phys.*, 2013, **51**, 1736–1742.
74 B. Gupta, M. Staub, G. G. Scherer and D. Grman, *J. Polym. Sci., Part A: Polym. Chem.*, 1995, **33**, 1545–1549.
75 J. Mališ, P. Mazúr, M. Paidar, T. Bystron and K. Bouzek, *Int. J. Hydrogen Energy*, 2016, **41**, 2177–2188.
76 M. Faraj, M. Boccia, H. Miller, F. Martini, S. Borsacchi, M. Geppi and A. Pucci, *Int. J. Hydrogen Energy*, 2012, **37**, 14992–15002.
77 C. Yang, S. Wang, W. Ma, L. Jiang and G. Sun, *J. Membr. Sci.*, 2015, **487**, 12–18.
78 R. V. Law, D. C. Sherrington, C. E. Snape, I. Ando and H. Korosu, *Ind. Eng. Chem. Res.*, 1995, **34**, 2740–2749.
79 G. H. Penner, R. Webber and L. A. O'Dell, *Can. J. Chem.*, 2011, **89**, 1036–1046.
80 T. Takewaki, L. W. Beck and M. E. Davis, *Microporous Mesoporous Mater.*, 1999, **33**, 197–207.
81 K. K. Laali, A. Jamalian and C. Zhao, *Tetrahedron Lett.*, 2014, **55**, 6643–6646.
82 L. Ghassemzadeh, M. Marrony, R. Barrera, K. D. Kreuer, J. Maier and K. Müller, *J. Power Sources*, 2009, **186**, 334–338.
83 B. Wang, W. Sun, F. Bu, X. Li, H. Na and C. Zhao, *Int. J. Hydrogen Energy*, 2016, **41**, 3102–3112.
84 T. M. Alam, M. Celina, R. A. Assink, R. L. Clough and K. T. Gillen, *Radiat. Phys. Chem.*, 2001, **60**, 121–127.
85 V. Maemets and I. Koppel, *J. Chem. Soc., Faraday Trans.*, 1997, **93**, 1539–1542.

86 P. Balakrishnan, A. L. Baumstark and D. W. Boykin, *Tetrahedron Lett.*, 1984, **25**, 169–172.
87 D. Boykin, *17O NMR Spectroscopy in Organic Chemistry*, CRC Press, USA, 1990.
88 I. P. Gerothanassis, *Prog. Nucl. Magn. Reson. Spectrosc.*, 2010, **56**, 95–197.
89 X. Wang and D. Z. Wang, *Tetrahedron*, 2011, **67**, 3406–3411.
90 M. Sankar, E. Nowicka, E. Carter, D. M. Murphy, D. W. Knight, D. Bethell and G. J. Hutchings, *Nat. Commun.*, 2014, **5**, 1–6.
91 W. G. Klemperer, *Angew. Chem., Int. Ed. Engl.*, 1978, **17**, 246–254.
92 J.-P. Kintzinger, in *Oxygen-17 and Silicon-29*, Springer Berlin Heidelberg, Berlin, Heidelberg, 1981, pp. 1–64, DOI: 10.1007/978-3-642-87762-9_1.
93 J. V. Gulmine, P. R. Janissek, H. M. Heise and L. Akcelrud, *Polym. Test.*, 2002, **21**, 557–563.
94 G. Socrates, *Infrared Characteristic Group Frequencies: Tables and Charts*, John Wiley & Sons, England,2nd edn, 1994.
95 M. M. Nasef, H. Saidi and K. Z. M. Dahlan, *Radiat. Phys. Chem.*, 2003, **68**, 875–883.
96 Y. Zhao, H. Yu, D. Xing, W. Lu, Z. Shao and B. Yi, *J. Membr. Sci.*, 2012, **421–422**, 311–317.
97 J. Fang, Y. Yang, X. Lu, M. Ye, W. Li and Y. Zhang, *Int. J. Hydrogen Energy*, 2012, **37**, 594–602.
98 H. Liu, S. Yang, S. Wang, J. Fang, L. Jiang and G. Sun, *J. Membr. Sci.*, 2011, **369**, 277–283.
99 R. B. Viana, A. B. F. da Silva and A. S. Pimentel, *Adv. Phys. Chem.*, 2012, **2012**, 14.
100 N. V. Venkataraman and S. Vasudevan, *J. Phys. Chem. B*, 2001, **105**, 1805–1812.
101 K. M. Harmon and I. Gennick, *Inorg. Chem.*, 1975, **14**, 1840–1845.
102 N. G. Sahoo, H. Bao, Y. Pan, M. Pal, M. Kakran, H. K. F. Cheng, L. Li and L. P. Tan, *Chem. Commun.*, 2011, **47**, 5235–5237.
103 A. Hasaninejad, M. Shekouhy, N. Golzar, A. Zare and M. M. Doroodmand, *Appl. Catal., A*, 2011, **402**, 11–22.
104 A. Filpi, M. Boccia, A. Pucci and F. Ciardelli, *e-Polym.*, 2013, **13**, 1–14.
105 V. I. Kovalenko, A. A. Akhmadiyarov, A. E. Vandyukov and A. R. Khamatgalimov, *J. Mol. Struct.*, 2012, **1028**, 134–140.
106 C. O. Laoire, S. Mukerjee, K. M. Abraham, E. J. Plichta and M. A. Hendrickson, *J. Phys. Chem. C*, 2009, **113**, 20127–20134.
107 Y.-F. He, R.-M. Wang, Y.-Y. Liu, Y. Chang, Y.-P. Wang, C.-G. Xia and J.-S. Suo, *J. Mol. Catal. A: Chem.*, 2000, **159**, 109–113.
108 I. Di Somma, R. Andreozzi, M. Canterino, V. Caprio and R. Sanchirico, *AIChE J.*, 2008, **54**, 1579–1584.